Tailoring Bose-Einstein-condensate environments for a Rydberg impurity

S. Rammohan,[1,*] A. K. Chauhan,[1,2] R. Nath,[3] A. Eisfeld,[4] and S. Wüster[1]

[1]*Department of Physics, Indian Institute of Science Education and Research, Bhopal, Madhya Pradesh 462 023, India*[†]

[2]*Department of Optics, Faculty of Science, Palacký University, 17 listopadu 1192/12, 77146 Olomouc, Czech Republic*

[3]*Department of Physics, Indian Institute of Science Education and Research, Pune 411 008, India*

[4]*Max Planck Institute for the Physics of Complex Systems, Nöthnitzer Strasse 38, 01187 Dresden, Germany*

(Received 24 November 2020; revised 9 May 2021; accepted 26 May 2021; published 15 June 2021)

Experiments have demonstrated that the excitation of atoms embedded in a Bose-Einstein condensate to Rydberg states is accompanied by phonon creation. Here we provide the theoretical basis for the description of phonon-induced decoherence of the superposition of two different Rydberg states. To this end, we determine Rydberg-phonon coupling coefficients using a combination of analytical and numerical techniques. From these coefficients, we calculate bath correlation functions, spectral densities, and reorganization energies. These quantities characterize the influence of the environment and form essential inputs for followup open quantum system approaches. We find that the amplitude of bath correlations scales like the power law ν^{-6} with the principal quantum number ν, while reorganization energies scale exponentially, reflecting the extreme tunability of Rydberg atomic properties.

DOI: 10.1103/PhysRevA.103.063307

I. INTRODUCTION

A growing arena in ultracold atomic physics is the study of impurities in quantum many-body systems. Here a minority species composed of ions [1–5], different elements [6], or molecules [7] is embedded in a majority species that may form a Bose-Einstein condensate (BEC) [2,3,8], thermal gas [9], or degenerate Fermi gas [10,11]. Besides the fundamental atomic physics interest, such experiments allow controlled tests of condensed matter impurity phenomena, ranging from the Kondo effect [12,13] over Polaron formation [14–18] to the Anderson orthogonality catastrophe [19].

While in the above examples the impurity typically is a particle in its electronic ground state, the impurity can also be a Rydberg excited atom of the same or another atomic species as the cold gas [20–23]. Rydberg atoms complement the above list of impurities in that they can interact equally strongly with a large but finite volume of the host medium, rather than dominantly with nearest neighbor atoms. The range and strength of interactions is further highly controllable through the choice of the Rydberg quantum state. Being neutral, Rydberg atoms are not too sensitive to stray external fields, while they still can be guided by controlled external fields. However, being electronically excited, they suffer spontaneous decay. The resulting lifetimes of tens or hundreds of microseconds [24,25] are much shorter than the millisecond timescales characteristic of BEC dynamics. We show in this article that interesting joint dynamics may arise between the two, despite this apparent timescale mismatch.

We focus on electronic dynamics of a single immobile Rydberg excited impurity atom embedded in a Bose-Einstein condensate. After rewriting the Hamiltonian in the form of a spin-boson model (SBM), we proceed to explicitly calculate the relevant Rydberg-phonon coupling constants. Focusing further on the case of two low-lying angular momentum states ($l = 0, 1$), we infer bath correlation functions, spectral densities, and re-organization energies to characterize the phonon environment. It turns out that the latter is highly tunable through Rydberg state quantum numbers and BEC phonon-mode structure.

In our setup, the environment is naturally initialized in a coherent initial state, instead of the usual vacuum or thermal state. This happens due to the sudden Rydberg excitation within a ground-state, zero-temperature BEC, resulting in a quench of the system. A similar scenario is encountered for vibrational dynamics of molecules following photoexcitation [26]. Many open-quantum system techniques are formulated for environments in an initial vacuum or thermal state. These can still be used here since the dynamics for an environment in a coherent initial state can be mapped onto one for the

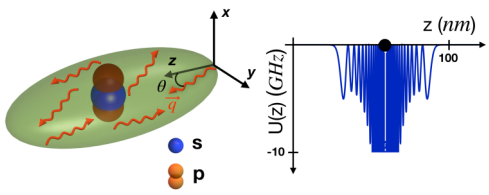

FIG. 1. Sketch of a Rydberg impurity in a BEC environment. (Left) A single Rydberg impurity in either of two selected internal states (s, p) couples to a large volume (blue or orange) of an embedding BEC (green), exciting phonons with wave vector $\mathbf{q}$ (red arrows). The shape of the coupling volume strongly differs in the two Rydberg electronic states. (Right) The system-environment coupling potential U has a peculiar oscillatory long-range character. For illustration, we sketch U for an impurity in state $|s\rangle$, cutoff at large $|U|$ for better visibility, along an arbitrary axis, here z.

*sidharth16@iiserb.ac.in

†sebastian@iiserb.ac.in

environment in a vacuum initial state but adding auxiliary terms in the system Hamiltonian.

Our results then form the basis for quite general treatment of Rydberg electronic state decoherence in BEC. For a simple case, they are validated by comparison with conceptually more straightforward solutions of the Gross-Pitaveskii equation in a companion article [27]. We also show there that the Rydberg atom in a BEC represents a particularly accessible example of an open quantum system where both the system *and* the environment can be interrogated in detail. The results may have further applications for the design of hybrid quantum technologies based on Rydberg atoms and BEC and creating flexible quantum simulation platforms for energy transport [28,29].

BEC-phonon-induced impurity decoherence has so far been mainly studied in the context of ground-state impurities of a minority species [8,17,18,30–38], ions [39], or polaron formation [40]. For ground-state impurities, spectral densities were reported in Ref. [41].

This article is organized as follows: First, we divide the many-body Hamiltonian in Sec. II into parts describing the system, the environment, and the coupling between the two. Then in Sec. III, within an open quantum system approach, we calculate environment correlation functions as well as spectral densities and then explore the scaling of the latter with principal quantum number. Finally, we conclude along with an outlook in Sec. IV. Details of calculations are provided in a set of Appendixes, with the incorporation of Bogoliubov excitations in the system environment coupling in Appendix A, calculation of the ensuing coupling constants in Appendix B, transformation of a coherent state environment into a vacuum one in Appendix C, details on correlation functions in Appendix D, and details on spectral densities in Appendix E.

II. INTERACTING MULTISPECIES SYSTEM

We begin with the many-body Hamiltonian $\hat{H}$ for a collection of bosonic atoms of mass m. The internal states of the atoms are denoted by k. This label k can, for example, correspond to the electronic ground state $|g\rangle$ or to a collection of Rydberg states $|\alpha\rangle = |\nu, l, m\rangle$, with principal quantum number ν, angular momentum l, and azimuthal quantum number m.

Using the field operator in the Heisenberg picture $\hat{\Psi}_k(\mathbf{x})$, which destroys an atom at location $\mathbf{x}$ in internal state k, we have

$$\hat{H} = \sum_k \int d^3\mathbf{x} \Big[\hat{\Psi}_k^\dagger(\mathbf{x}) \Big(-\frac{\hbar^2}{2m}\nabla^2 + E_k \Big) \hat{\Psi}_k(\mathbf{x}) + \frac{1}{2} \sum_{i,j,s} \int d^3\mathbf{y} \hat{\Psi}_k^\dagger(\mathbf{x}) \hat{\Psi}_i^\dagger(\mathbf{y}) U_{kijs}(\mathbf{x}-\mathbf{y}) \hat{\Psi}_j(\mathbf{y}) \hat{\Psi}_s(\mathbf{x}) \Big]. \tag{1}$$

The first line of the Hamiltonian (1) are single-particle energies: kinetic energy and internal electronic energies E_k. We do not consider any external potential. The second term contains interatomic interactions, which may be long range due to the presence of Rydberg states and where we have allowed for interactions to change the internal state.

We now focus on the scenario of a single Rydberg impurity that is allowed to occupy multiple electronic states, which is embedded in a majority BEC with atoms in the ground state. Exploiting these constraints, we proceed in the following subsections to split the general Hamiltonian (1) into the three pieces that enter an open quantum system treatment [42–44], namely the sub-Hamiltonians for the quantum system (Rydberg atom states), the environment (BEC), and the system-environment coupling, respectively:

$$\hat{H} = \hat{H}_{\rm syst} + \hat{H}_{\rm env} + \hat{H}_{\rm coup}. \tag{2}$$

Based on this segregation, we are able to evaluate the essential inputs for any open-quantum system approach, which are environment correlation functions or spectral densities.

A. Rydberg quantum system

To make the above field operator notation compatible with the more usual formalism employed in Rydberg physics, we assume a highly localized Rydberg atom, restricting its position to a single, immobile spatial mode. We thus write

$$\hat{\Psi}_\alpha(\mathbf{x}) \approx \varphi_0(\mathbf{x}) \hat{a}^{(\alpha)}, \tag{3}$$

where $\hat{a}^{(\alpha)}$ creates a particle from the vacuum with internal state α and spatial mode $\varphi_0(\mathbf{x})$. For the Rydberg atom, multiple internal electronic states $|\,\alpha\,\rangle = |\,\nu, l, m\,\rangle$, defined above, are available. In the following, we shall use the Greek indices α, β, with $|\,\beta\,\rangle = |\,\nu', l', m'\,\rangle$ to refer to two such complete sets of quantum numbers.

For a single Rydberg impurity, with the identification $\hat{a}^{\dagger(\nu l m)} \hat{a}^{(\nu' l' m')} \leftrightarrow |\,\nu l m\,\rangle\langle\,\nu' l' m'\,|$, we thus reach the simple system Hamiltonian

$$\hat{H}_{\rm syst} = \sum_{\nu l m} E_{\nu l m} |\,\nu l m\,\rangle\langle\,\nu l m\,|, \tag{4}$$

where $E_{\nu l m}$ are the single-atom energies corresponding to the state $|\,\nu l m\,\rangle$, which can be found with standard methods [45]. Since we assume a localized Rydberg atom $\varphi_0(\mathbf{x}) \approx \delta^{(3)}(\mathbf{x} - \mathbf{R})$ at rest, we ignore its kinetic energy operator in Eq. (1). Here $\delta^{(3)}$ is the three-dimensional delta function.

We shall see later that as usual the coupling to the BEC environment introduces energy shifts that are formally best included in $\hat{H}_{\rm syst}$ as well, so that in Appendix B 6 we define a modified system Hamiltonian $\hat{H}'_{\rm syst}$; see Eq. (B23).

B. Condensate environment

For the ground-state atoms ($k = g$) that form the BEC, the Hamiltonian (1) becomes

$$\hat{H} = \int d^3\mathbf{x} \Big[\hat{\Psi}_g^\dagger(\mathbf{x}) \Big(-\frac{\hbar^2}{2m}\nabla^2 + E_g \Big) \hat{\Psi}_g(\mathbf{x}) + \frac{U_0}{2} \hat{\Psi}_g^\dagger(\mathbf{x}) \hat{\Psi}_g^\dagger(\mathbf{x}) \hat{\Psi}_g(\mathbf{x}) \hat{\Psi}_g(\mathbf{x}) \Big], \tag{5}$$

assuming the usual s-wave contact interactions [46]

$$U_{gggg}(\mathbf{x}-\mathbf{y}) = U_0 \delta^{(3)}(\mathbf{x}-\mathbf{y}), \tag{6}$$

with $U_0 = 4\pi\hbar^2 a_s/m$, where a_s is the s-wave atom-atom scattering length.

We split the ground-state field operator as usual [46],

$$\hat{\Psi}_g(\mathbf{x}) = \phi_0(\mathbf{x}) + \hat{\chi}(\mathbf{x}), \tag{7}$$

where $\phi_0(\mathbf{x}) \in \mathbb{C}$ is the mean-field condensate wave function and $\hat{\chi}(\mathbf{x})$ is the fluctuation operator which we expand as

$$\hat{\chi}(\mathbf{x}) = \sum_{\mathbf{q}} (u_{\mathbf{q}}(\mathbf{x})\hat{b}_{\mathbf{q}} - v^*_{\mathbf{q}}(\mathbf{x})\hat{b}^\dagger_{\mathbf{q}}) \tag{8}$$

in terms of Bogoliubov–de Gennes (BdG) excitations. In a homogenous BEC with number density $\rho = |\phi_0|^2$, these have mode functions $u_{\mathbf{q}}(\mathbf{x}) = \bar{u}_q \exp[i\mathbf{q}\cdot\mathbf{x}]/\sqrt{\mathcal{V}}$ and $v_{\mathbf{q}}(\mathbf{x}) = \bar{v}_q \exp[i\mathbf{q}\cdot\mathbf{x}]/\sqrt{\mathcal{V}}$ with bosonic creation and destruction operators $\hat{b}^\dagger_{\mathbf{q}}$ and $\hat{b}_{\mathbf{q}}$, assuming a box quantization volume $\mathcal{V}$. Here and in the following, we use subscripts q for quantities that only depend on the modulus of the quasiparticle wave number. The BdG mode amplitudes are $\bar{u}_q = [(\zeta_q/\epsilon_q + 1)/2]^{1/2}$ and $\bar{v}_q = [(\zeta_q/\epsilon_q - 1)/2]^{1/2}$, with $\zeta_q = \epsilon_q + \rho U_0$, where $q = |\mathbf{q}|$ and

$$\epsilon_q = \hbar\omega_q = \sqrt{\frac{\hbar^2 q^2}{2m}\left(\frac{\hbar^2 q^2}{2m} + 2U_0\rho\right)}, \tag{9}$$

are the BdG mode energies. The BdG amplitudes fulfill $\bar{u}_q^2 - \bar{v}_q^2 = 1$ and $\lim_{q\to\infty}\bar{u}_q = 1$, $\lim_{q\to\infty}\bar{v}_q = 0$ with $\lim_{q\to 0}\bar{u}_q - \bar{v}_q = 0$.

Inserting (7) and (8) into the Hamiltonian (5) for the state $|\,g\,\rangle$ then as usual gives rise to the Hamiltonian

$$\hat{H}_{\rm env} = E_{\rm GP}[\phi_0(\mathbf{x})] + \sum_{\mathbf{q}} \epsilon_q \hat{b}^\dagger_{\mathbf{q}}\hat{b}_{\mathbf{q}}, \tag{10}$$

where $E_{\rm GP}[\phi_0(\mathbf{x})]$ is the Gross-Pitaevskii energy functional

$$E_{\rm GP}[\phi_0(\mathbf{x})] = \int d^3\mathbf{x}\Big[-\frac{\hbar^2}{2m}|\nabla\phi_0(\mathbf{x})|^2 + E_g|\phi_0(\mathbf{x})|^2 + \frac{U_0}{2}|\phi_0(\mathbf{x})|^4\Big]. \tag{11}$$

C. System-environment interactions

The main interest is in the system-environment coupling Hamiltonian $\hat{H}_{\rm coup}$. Since we already dealt with interactions of ground-state atoms in Sec. II B and focus on at most one Rydberg excitation in the present article, the only remaining combinations of indices $kijs$ in the interaction part of the Hamiltonian (1) must involve one or two Rydberg indices only. We can exclude all terms that would involve transitions between ground and Rydberg states, due to the large energy difference and small wave-function overlap of the impurity ground-state wave function and the BEC. Considering these constraints, the only required index sets are $kijs = g\alpha\beta g$ and $kijs = \alpha gg\beta$, which describe the interaction of a ground state with a Rydberg atom, possibly changing the internal state of the latter.

The dominant mechanism by which Rydberg atoms can interact with ground-state atoms is through elastic scattering between the Rydberg electron and ground-state atoms, once the latter venture into the Rydberg orbit [47]. This is described by the Fermi pseudopotential

$$V(\mathbf{y}+\mathbf{r},\mathbf{x}) = g_0\delta^{(3)}(\mathbf{y}+\mathbf{r}-\mathbf{x}), \tag{12}$$

where $g_0 = 2\pi\hbar^2 a_e/m_e$ [48]. Here, a_e is the electron-atom scattering length with $a_e < 0$ for Sr and Rb and m_e is the electron mass. We have split the absolute position of the Rydberg electron $\mathbf{y}+\mathbf{r}$ into the location of the ion core of the Rydberg atom $\mathbf{y}$, and the relative displacement of its electron $\mathbf{r}$. Interactions require the location of the electron to co-incide with that of a ground-state atom at $\mathbf{x}$. We neglect for simplicity the slight momentum dependence of the electron-atom scattering length a_e (see, e.g., Ref. [49]), as well as the effect of the direct interaction with the ion core, which is relevant in a small BEC volume only [50,51]. The latter is also independent of electronic state and hence not expected to contribute to decoherence.

In order to incorporate the potential (12), the Hamiltonian (1) could be written in terms of an explicit Rydberg electron position, as has been analyzed in Ref. [52]. Since energy differences between Rydberg states are much larger than the typical interaction energy scales with ground-state atoms, it is frequently useful to revert back to the atomic energy basis for the Rydberg electron, which we do here. Since we consider only a single impurity and $[\hat{\Psi}_\alpha(\mathbf{x}), \hat{\Psi}_\beta(\mathbf{y})] = 0$, the system-environment interaction part of (1) finally boils down to

$$\hat{H}_{\rm int} = \sum_{\alpha,\beta}\int d^3\mathbf{x}\int d^3\mathbf{y} \times \hat{\Psi}^\dagger_g(\mathbf{x})\hat{\Psi}^\dagger_\alpha(\mathbf{y})U^{g\alpha\beta g}(\mathbf{x}-\mathbf{y})\hat{\Psi}_\beta(\mathbf{y})\hat{\Psi}_g(\mathbf{x}). \tag{13}$$

with long-range ground-state Rydberg atom interaction

$$U^{g\alpha\beta g}(\mathbf{x}-\mathbf{y}) = g_0[\psi^{(\alpha)*}(\mathbf{x}-\mathbf{y})\psi^{(\beta)}(\mathbf{x}-\mathbf{y})]. \tag{14}$$

Here $\psi^{(\alpha)}(\mathbf{r})$ denotes the electronic wave function of the Rydberg electron in quantum state $|\,\alpha\,\rangle$ at a separation $\mathbf{r}$ from the core. The position $\mathbf{y}$ in (14) is that of the core of the Rydberg atom and $\mathbf{x}$ is that of a ground-state atom. For $\alpha = \beta$, the term (14) hence describes the energy shifts of Rydberg and ground-state atoms due to their proximity, while for $\alpha \neq \beta$ it allows the possibility that scattering from ground-state atoms causes a Rydberg state transition. The range of the interaction (14) is the extent of the Rydberg wave function ψ, which is slightly larger than the mean orbital radius $r_{\rm orb} \approx 3a_0\nu^2/2$, where a_0 is the Bohr radius.

We now insert Eqs. (7) and (8) into the ground-state–Rydberg-state interaction Hamiltonian (13) containing (14) and assume the core of the Rydberg atom to be very tightly localized in a single mode at the origin, using Eq. (3). We give some more details on intermediate steps, as well as some initial steps for an inhomogenous condensate in Appendix A.

After defining a splitting of the interaction Hamiltonian according to

$$\hat{H}_{\rm int} = \sum_{\alpha\beta}\hat{S}^{(\alpha\beta)}\otimes\hat{B}^{(\alpha\beta)} \tag{15}$$

into system parts $\hat{S}^{(\alpha\beta)} = \hat{a}^{(\alpha)\dagger}\hat{a}^{(\beta)}$ and environment parts $\hat{B}^{(\alpha\beta)}$ and focusing on the case of a spatially homogeneous condensate with real mean field $\phi_0 \approx \sqrt{\rho}$, where ρ is the

number density, we find

$$\hat{B}^{(\alpha\beta)} = \left[\bar{E}^{(\alpha\beta)} + \sum_{\mathbf{q}} \left(\kappa_{\mathbf{q}}^{*(\alpha\beta)} \hat{b}_{\mathbf{q}}^{\dagger} + \kappa_{\mathbf{q}}^{(\alpha\beta)} \hat{b}_{\mathbf{q}}\right)\right], \tag{16}$$

with mean-field shift

$$\bar{E}^{(\alpha\beta)} = g_0 \int d^3\mathbf{x}\ |\phi_0(\mathbf{x})|^2 \psi^{*(\alpha)}(\mathbf{x}) \psi^{(\beta)}(\mathbf{x}) \tag{17}$$

and system-phonon coupling

$$\kappa_{\mathbf{q}}^{(\alpha\beta)} = g_0 \sqrt{\rho} \int d^3\mathbf{x}\ \psi^{*(\alpha)}(\mathbf{x}) \psi^{\beta}(\mathbf{x}) [u_{\mathbf{q}}(\mathbf{x}) - v_{\mathbf{q}}^{*}(\mathbf{x})]. \tag{18}$$

After adding (17) to $E_{\mathrm{GP}}[\phi_0(\mathbf{x})]$, one can already use the Gross-Pitaevskii equation (GPE) to study the mean-field dynamics of the condensate in the presence of a Rydberg impurity in a single state α. One important effect in that case is imprinting of a phase onto the condensate wave function in any region where condensate atoms feel $U^{g\alpha\alpha g}$ [53,54]. This allows, for example, tracking of a mobile Rydberg impurity [55] or distinguishing different electronic states [54]. In a homogenous system as we consider here, $\bar{E}^{(\alpha\beta)} = g_0 \rho\, \delta_{\alpha,\beta}$, which causes an energy shift that, e.g., can be utilized to locate the Rydberg excitation in a specific density region of the BEC [21,56]. For Sr atoms with density 4.9×10^{20} m^{-3}, we would have $\bar{E}^{(ss)} = -54$ MHz. In an inhomogeneous background (not further considered here), the term provides an effective potential exerting a force on the Rydberg impurity [55,57].

While the results so far were general, from now on we consider the principal quantum number of both the Rydberg states, ν and ν', to be equal for simplicity. Then, for α, β with $l = 0$ and $l' = 0$, denoted $(\alpha\beta) = (ss)$, the expression (18) can be calculated analytically and has been used in Refs. [21,58] to understand atom loss through repeated excitation of Rydberg impurities in a BEC; we list the result in Appendix B. We approximate Rydberg electron wave functions by those for hydrogen in the following, which should be a good approximation at large ν. One finds that $\kappa_{\mathbf{q}}^{(ss)}$ depends on $q = |\mathbf{q}|$ only, with functional dependence shown in Fig. 2(a). For demonstrations in this section, we consider the Rydberg impurity at the origin, in a ^{84}Sr condensate with density $\rho = 4.9 \times 10^{20}$ m^{-3}, and hence use the corresponding atom electron scattering length $a_e = -18 a_0$ [59], the atomic mass $m = 1.393 \times 10^{-25}$ kg, and atom-atom scattering length $a_s = 122.7 a_0$ [60]. The coupling coefficients still depend on the mode quantisation volume (we used $\mathcal{V} = 204\ \mu$m^3), defined after Eq. (11). $\mathcal{V}$ will drop out in subsequent results. We show the dependence of couplings on wave number multiplied by healing length $\xi = 1/(2\sqrt{2\pi a_s \rho})$. Then $q\xi \lesssim 1$ corresponds to the phonon part of the BEC excitation spectrum and the higher wavenumbers to the free particle one. For the parameters above, $\xi = 0.11\ \mu$m.

As discussed in the supplement of Ref. [21], the dominant peak in $\kappa_{\mathbf{q}}^{(ss)}$, representing the largest value of the system-environment coupling, occurs at wave numbers determined by the size of the Rydberg orbit $q \approx 2/r_{\mathrm{orb}}$ and lies in the regime of phonon excitations, as seen by comparison with the BdG dispersion relation shown as red dashed line in Fig. 2. Further equally spaced peaks with alternating sign follow

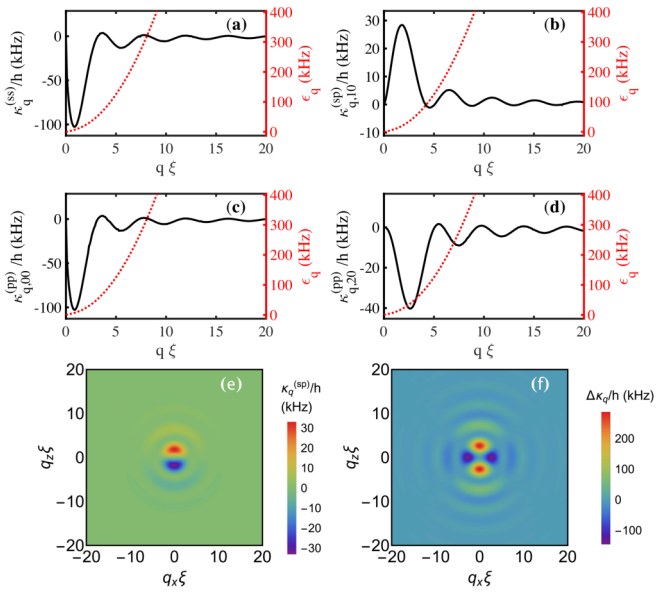

FIG. 2. Overview of Rydberg-phonon coupling constants for a single impurity with $\nu = 40$. (a) The coupling $\kappa_q^{(ss)}$ of state $|\,s\,\rangle$ to a phonon with wave number q is isotropic due to the symmetry of the Rydberg wave function. The right axis shows the phonon dispersion relation (9) for orientation. (b) In contrast, the transition coupling $\kappa_{q,10}^{(sp)}$ between $|\,s\,\rangle$ and $|\,p\,\rangle$ is anisotropic, since it involves $|\,p\,\rangle$ states. (c) Isotropic component $\kappa_{q,00}^{(pp)}$ of coupling in the state $|\,p\,\rangle$. (d) Anisotropic component $\kappa_{q,20}^{(pp)}$ of coupling in the state $|\,p\,\rangle$. (e) Transition coupling $\kappa_q^{(sp)}$ in the q_x, q_z plane. (f) The difference of couplings $\Delta\kappa_{\mathbf{q}} = \kappa_q^{(pp)} - \kappa_q^{(ss)}$ will be most relevant for Rydberg decoherence.

at wave numbers $q \geqslant 1/\xi$ for which BEC excitations have single-particle character.

When $l = 1$ or $l' = 1$, the integrand in (18) is no longer isotropic. To be specific, we restrict the present work to azimuthal quantum numbers $m = 0$ assuming the quantization axis along the z direction. Removing other m states from the picture can typically be achieved by additional Zeeman shifts through an external bias magnetic field [61,62]. The resultant coupling will then depend on the angle θ between the propagation direction of the phonon, $\mathbf{q}$, and the quantization axis, sketched in Fig. 1. It turns out that the angular dependence is described using just two spherical harmonics Y_{lm} as $\kappa_{\mathbf{q}}^{(\alpha\beta)} = \kappa_{q,00}^{(\alpha\beta)}(q) Y_{00} + \kappa_{q,20}^{(\alpha\beta)}(q) Y_{20}(\theta)$, where $\kappa_{q,00}^{(\alpha\beta)}$ and $\kappa_{q,20}^{(\alpha\beta)}$ are the isotropic and anisotropic parts of the coupling, respectively.

As described in Appendix B, we perform the angular integration contained in (18) analytically and the subsequent one over the radial variable $r = |\mathbf{x}|$ numerically. The results of this procedure are also shown in Fig. 2. We see as in the case of $\kappa_{\mathbf{q}}^{(ss)}$ that the coupling to condensate excitations when p states are involved has an oscillatory dependence on the excitation wave number and extends over both the phonon and the single-particle part of the spectrum. We will see shortly that the difference between couplings in the s and p states, shown in Fig. 2(f), will be most relevant for studies of decoherence, since it encapsulates the ability of the BEC environment to "measure" the electronic state of the Rydberg system.

III. OPEN QUANTUM SYSTEM APPROACH

If one is not interested in all degrees of freedom of a complex quantum system, it is convenient to split it into a system $\mathcal{S}$ and an environment $\mathcal{E}$, and then investigate the quantum dynamics of the system only. Formally, the latter is given by

$$\hat{\rho}_{\mathcal{S}}(t) = \mathrm{Tr}_{\mathcal{E}}(\hat{U}(t)[\hat{\rho}_{\mathcal{S}}(0) \otimes \hat{\rho}_{\mathcal{E}}(0)]\hat{U}^{\dagger}(t)), \tag{19}$$

where $\hat{\rho}_{\mathcal{S}}(t)$ is the reduced density matrix of the system, $\mathrm{Tr}_{\mathcal{E}}$ denotes the trace over the environmental degrees of freedom, $\hat{U}(t)$ is the time evolution operator of the complete system, and $\hat{\rho}_{\mathcal{S},\mathcal{E}}(0)$ are the initial reduced density matrices of system and environment, respectively. Since (19) is still based on the time-evolution operator of the complete system, it still contains the full complexity of the problem.

Open quantum system techniques aim to remove part of that complexity by finding an evolution equation that does not require us to solve explicitly the bath degrees of freedom, but instead directly evolves

$$\hat{\rho}_{\mathcal{S}}(t) = \sum_{ss'} \rho_{ss'}(t)|\, s\,\rangle\langle\, s'\,|, \tag{20}$$

with $s, s' \in \{s, p\}$. The effect of the environment enters the evolution equation for (20) through certain correlation functions, which we discuss for our case in Sec. III A. If this effect remembers the past evolution of $\hat{\rho}_{\mathcal{S}}(t)$, we talk about a non-Markovian system; otherwise we denote it as a Markovian one [42,43].

With the identification $|\uparrow\rangle = |\, p\,\rangle$ and $|\downarrow\rangle = |\, s\,\rangle$ and constraining the Rydberg system to these two electronic states, we show in Appendix B 6 how the total Hamiltonian for our system can be rewritten as

$$\hat{H}_{\mathrm{tot}} = \hat{H}'_{\mathrm{syst}} + \sum_{\mathbf{q}} \hbar\omega_q\, \tilde{b}^{\dagger}_{\mathbf{q}}\tilde{b}_{\mathbf{q}} + \sum_{\mathbf{q}} \frac{\Delta\kappa_{\mathbf{q}}}{2}(\tilde{b}_{\mathbf{q}} + \tilde{b}^{\dagger}_{\mathbf{q}})\hat{\sigma}_z + i\sum_{\mathbf{q}} \kappa^{(sp)}_{\mathbf{q}}(\tilde{b}_{\mathbf{q}} - \tilde{b}^{\dagger}_{\mathbf{q}})\hat{\sigma}_y + \mathrm{const.}, \tag{21}$$

with $\Delta\kappa_{\mathbf{q}} = \kappa^{(pp)}_q - \kappa^{(ss)}_q$. In (21), the environmental oscillator frequencies ω_q are set by the BdG mode energies in (9). The coefficients κ are defined in Eq. (18) and the caption of Fig. 2, and $\hat{\sigma}_{y,z}$ are the usual Pauli spin operators. We recognize (21) as a variant of the well-known spin-boson model (SBM) [63,64], with one term that describes energy gap fluctuations of the spin ($\sim\hat{\sigma}_z$) and one describing incoherent spin flips ($\sim\hat{\sigma}_y$).

The first term in Eq. (21) is essentially Eq. (4), with minor energy shifts due to system-environment coupling discussed in Appendix B 6. The BdG excitations in the second term created by $\tilde{b}^{\dagger}$ correspond to shifted harmonic oscillator modes,

$$\tilde{b}_{\mathbf{q}} = \hat{b}_{\mathbf{q}} + \frac{\bar{\kappa}_{\mathbf{q}}}{2\hbar\omega_q}, \tag{22}$$

$$\tilde{b}^{\dagger}_{\mathbf{q}} = \hat{b}^{\dagger}_{\mathbf{q}} + \frac{\bar{\kappa}_{\mathbf{q}}}{2\hbar\omega_q}, \tag{23}$$

with $\bar{\kappa}_{\mathbf{q}} = \kappa^{(pp)}_{\mathbf{q}} + \kappa^{(ss)}_{\mathbf{q}}$, as discussed in detail in Appendix B 6. We assume a Bose-Einstein condensate at temperature $T = 0$ as initial state prior to Rydberg excitation, hence $\hat{\rho}_{\mathcal{E}}(0) = |\,0\,\rangle\langle\,0\,|$, where $|\,0\,\rangle$ is the Bogoliubov vacuum of the original unshifted quasiparticle operators: $\hat{b}_{\mathbf{q}}|\,0\,\rangle = 0$.

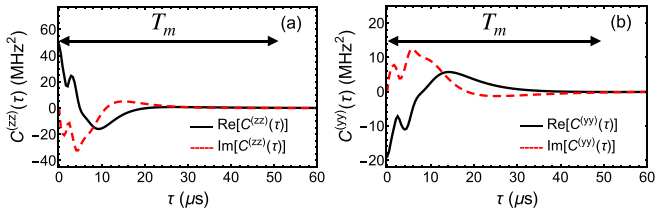

FIG. 3. Phonon correlation functions, defined in Eq. (28), for coupling to a Rydberg impurity with principal quantum number $\nu = 40$. (a) Re$[C^{(zz)}(\tau)]$ (black) and Im$[C^{(zz)}(\tau)]$ (red dashed); (b) $C^{(yy)}(\tau)$ with the same line styles. Other correlations vanish: $C^{(zy)}(\tau) = C^{(yz)}(\tau) = 0$.

For the operators $\tilde{b}_{\mathbf{q}}$, the initial state $\hat{\rho}_{\mathcal{E}}(0)$ corresponds to a many-mode coherent state as shown in Appendix B 6. This seems to be an obstacle for the application of open quantum system methods which require the environment initially to be in the vacuum state. However, as we demonstrate in Appendix C, the open quantum system evolution according to (19) from the coherent environment initial state is equivalent to evolution using a vacuum environment initial state with a modified time-dependent system Hamiltonian

$$\hat{H}''_{\mathrm{syst}} = \left[\frac{\Delta E}{2} + \sum_{\mathbf{q}} \frac{\Delta\kappa_{\mathbf{q}}\,\bar{\kappa}_{\mathbf{q}}}{2\hbar\omega_q}(\cos(\omega_q t) - 1)\right]\hat{\sigma}_z, \tag{24}$$

entering the open quantum system method. The method then additionally has to incorporate decoherence as usual. In (24), $\Delta E = E_p - E_s$ is the energy splitting between the $|\, p\,\rangle$ and the $|\, s\,\rangle$ state. For this, we have combined Eqs. (4), (B23), and (C3). Due to the equivalence discussed above, we shall thus consider the environment in the vacuum state also for the shifted operators $\tilde{b}_{\mathbf{q}}$, but using (24) for the system.

Finally, for later use, let us reformulate the interaction Hamiltonian within (21) as

$$\hat{H}_{\mathrm{int}} = \hat{\sigma}_z \otimes \hat{E}^{(z)} + \hat{\sigma}_y \otimes \hat{E}^{(y)}, \tag{25}$$

$$\hat{E}^{(z)} = \sum_{\mathbf{q}} \frac{\Delta\kappa_{\mathbf{q}}}{2}(\tilde{b}_{\mathbf{q}} + \tilde{b}^{\dagger}_{\mathbf{q}}), \tag{26}$$

$$\hat{E}^{(y)} = i\sum_{\mathbf{q}} \kappa^{(sp)}_{\mathbf{q}}(\tilde{b}_{\mathbf{q}} - \tilde{b}^{\dagger}_{\mathbf{q}}). \tag{27}$$

We shall in the following work out environmental properties such as correlation functions in terms of these new operators $\hat{E}^{(z)}$ and $\hat{E}^{(y)}$. As usual, the system environment interaction Hamiltonian leads to entanglement between system and environment and thus ultimately to decoherence of the system.

A. Single-impurity Bath correlation functions

In an approximate reduced description for the system, all effects of the environment can usually be taken into account through the environment correlation functions

$$C^{(kl)}(\tau) = \langle\, 0\,|\hat{E}^{(k)}(\tau)\hat{E}^{(l)}(0)|\,0\,\rangle, \tag{28}$$

where $k, l \in \{y, z\}$, operators are understood in the interaction picture, and $\tilde{b}_{\mathbf{q}}|\,0\,\rangle = 0$ as discussed above.

We show in Fig. 3 the relevant correlation functions for the two system-bath coupling operators $\hat{E}^{(z)}$, $\hat{E}^{(y)}$ in (21), for the

same parameters as in Fig. 2. The third possible correlation function $C^{(zy)}(\tau) = \langle \hat{E}^{(z)}(\tau)\hat{E}^{(y)}(0)\rangle$ vanishes. The calculations are described in more detail in Appendix D. We can already estimate typical decoherence timescales $T_{\rm decoh}$ for Rydberg electronic state superpositions from these results: It is known that decoherence of a superposition of eigenstates of σ_z (here the electronic states $|\,s\,\rangle$ and $|\,p\,\rangle$), will be dominated by the part of $\hat{H}_{\rm int}$ that depends on $\hat{\sigma}_z$ [65]. The timescale can thus be estimated as $T_{\rm decoh} \sim 1/\sqrt{2C^{(zz)}(0)}$ [65]. For the case of Fig. 3, we obtain $T_{\rm decoh} \approx 20$ ns. This is much shorter than the vacuum lifetime of $\nu = 40$ Rydberg states, about $\tau \approx 40\ \mu$s [66,67], or decoherence times in vacuum, which can be of the order of milliseconds even near surfaces [68]. The range of decoherence timescales $T_{\rm decoh}$ above also can easily be made faster than inelastic processes, which for present parameters would take place within 1–10 μs [56,67]. Decoherence times can be read out by subjecting a superposition of $|\,s\,\rangle$ and $|\,p\,\rangle$ to a strong, fast Rabi $\pi/2$ pulse on the sp transition. After the pulse, the population in, e.g., $|\,p\,\rangle$ will reflect the coherence density matrix element ρ_{sp} in Eq. (20) [69–71].

Another important aspect visible in Fig. 3 is the phonon environment memory time T_m, over which correlation functions drop to zero. Let us loosely refer to the characteristic timescale of the Rydberg impurity as $T_{\rm sys}$. This can be either given by the energy splitting between our two states $T_{\rm sys} \sim h/|E_\alpha - E_\beta|$, or if these are coupled by a microwave set by its Rabi frequency: $T_{\rm sys} \sim h/\Omega_{\rm mw}$. Then, for characteristic Rydberg system timescales $T_{\rm sys} \gg T_m$ we would expect Markovian open quantum system dynamics, for $T_{\rm sys} \leqslant T_m$ non-Markovian. We can read off from Fig. 3 that $T_m \approx 50\ \mu$s at $\nu = 40$. Dynamics of either kind discussed above can typically be faster, and hence we expect our system to be able to show non-Markovian features. It will in fact be difficult to generate a nontrivially evolving quantum system that is Markovian, since the Rydberg evolution time would be limited by the radiative lifetime, which even in vacuum is of the same order as T_m.

By inspecting the Hamiltonian (21), we see that $C^{(yy)}$ is related to phonon-induced transitions between Rydberg states. One would expect those to be strongly suppressed for phonon energies in the kHz range, and Rydberg energy splittings of GHz for energetic reasons. We confirm this expectation in Ref. [27].

B. Phonon spectral densities and environment tuning

To isolate temperature effects that are encoded in the environment initial state $\hat{\rho}_{\mathcal{E}}(0)$, from the features of the system-environment coupling, one also frequently considers the environment spectral density $J(\omega)$ that encapsulates the relevance of environmental degrees of freedom with frequency ω. In our case, spectral densities are defined as

$$J^{(z)}(\omega) = \sum_{\mathbf{q}} \frac{\Delta\kappa_{\mathbf{q}}^2}{4}\delta(\omega - \omega_{\mathbf{q}}), \tag{29}$$

$$J^{(y)}(\omega) = \sum_{\mathbf{q}} \kappa_{\mathbf{q}}^{(sp)2}\delta(\omega - \omega_{\mathbf{q}}). \tag{30}$$

Since our environment is in the vacuum state, these can also be written as the Fourier transform of the bath correlation functions in Sec. III A, via

$$J^{(z)}(\omega) = \frac{1}{2\pi}\int_0^\infty d\tau\, C^{(zz)}(\tau)e^{i\omega\tau}, \tag{31}$$

$$J^{(y)}(\omega) = \frac{1}{2\pi}\int_0^\infty d\tau\, C^{(yy)}(\tau)e^{i\omega\tau}. \tag{32}$$

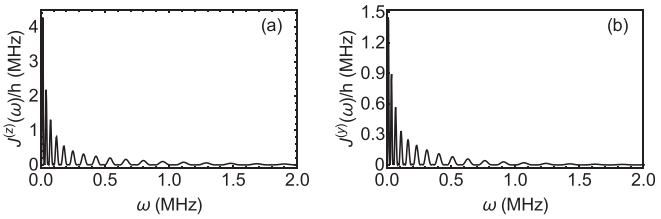

FIG. 4. Spectral properties of BEC phonon environment for a Rydberg impurity in $\nu = 120$. (a) Spectral density $J^{(z)}(\omega)$ and (b) $J^{(y)}(\omega)$. These are defined by Eqs. (29) and (30) or equivalently Eqs. (31) and (32).

The results are shown in Fig. 4, with details of the calculation in Appendix E. The spectral densities display a nontrival series of peaks and thus indicate the presence of a *structured environment*. The structure originates from that of the coupling constants $\kappa_{\mathbf{q}}$ in Fig. 2, since the spectral densities are found as Fourier transform of the Bath correlation functions C. These in turn are a type of inverse Fourier transform of the $\kappa_{\mathbf{q}}^2$ according to Eqs. (D4) and (D8). However, since one transform is in terms of the variable pair (ω, τ) and the other in term of $(\mathbf{q}, \tau)$, the peaks are now no longer equidistant, but stretched in accordance with the dispersion relation $\omega(\mathbf{q})$ (9).

Either spectral densities such as in Fig. 4 or bath correlation functions as in Fig. 3 now fully capture the effect of the condensate environment on the Rydberg impurity. Note that the bath correlation function at time zero, which entered the estimation of the decoherence time, is directly related to the integral over the corresponding spectral density. Given the extreme scaling of Rydberg electronic state properties with principal quantum number, we now expect a similar degree of tunability in the influence of the environment. To demonstrate that this is indeed the case, Fig. 5 shows how two measures for the impact of the environment on the system depend on the Rydberg principal quantum number ν.

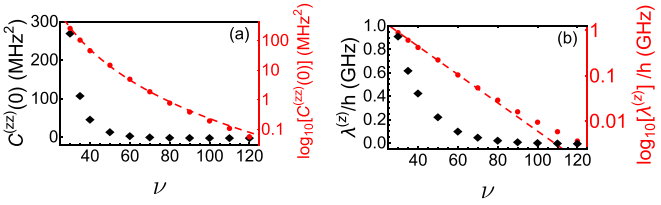

FIG. 5. Tuning of the condensate environment. (a) Variation of the bath auto-correlation function $C^{(zz)}(0)$ (black diamonds) as a function of principal quantum number ν along with the power-law fit $C^{(zz)}(0) = 1.25 \times 10^{11}\ \nu^{-6}$ MHz^2 as a red dashed line. We show both linear (black) and logarithmic (red) axes. (b) The reorganization energy $\lambda^{(z)}$, see Eq. (33), with the exponential fit $\lambda^{(z)} = 5.76 \times 10^3\ e^{-0.06\times\nu}$ GHz.

The first measure is the initial value of the bath correlation function $C(0)$, shown in Fig. 5(a), which scales as ν^{-6}. To understand this, note that neglecting the weak q dependence of $u_q - v_q$ allows one to write Eq. (18) as $\kappa_{\mathbf{q}}^{(\alpha\alpha)} \sim \mathcal{F}[|\psi(\mathbf{x})^{(\alpha\alpha)}](-\mathbf{q})$, where $\mathcal{F}$ denotes the Fourier transform. Using the convolution theorem, we can then show that $C(0) \sim \int d^3\mathbf{x}|\psi(\mathbf{x})|^4 \sim \nu^{-6}$. Another frequently used measure is the reorganization energy

$$\lambda^{(z)} = \int_0^\infty \frac{J^{(z)}(\omega)}{\omega} d\omega, \tag{33}$$

which is shown in Fig. 5(b). Large values for either quantity indicate a fast decohering effect of the environment. We can see that system-environment coupling can be tuned over orders of magnitude through the principal quantum number. Despite the wider excursions of the Rydberg electron into the ambient BEC medium for the higher principal quantum numbers, we find stronger system bath coupling at lower principal quantum numbers, because the stronger confinement of the Rydberg wave function at lower ν leads to a higher electron probability density, which in turn determines the coupling strength.

While we have focused here on the tuning of system-environment coupling through choice of Rydberg properties, an alternate route is a modification of the ambient condensate. We can see from Eq. (18) in conjunction with (28) or (30) that all quantities in Fig. 5 are multiplied with the BEC density ρ. The decoherence time estimates given in Sec. III A will scale like $T_{\text{decoh}} \sim \rho^{-1/2}$ due to this factor. Additionally, the condensate mean-field interaction strength U_0 and density enter the expression through the phonon energies $\epsilon_{\mathbf{q}}$ in (9) and BdG mode amplitudes. Interactions U_0 can be tuned using Feshbach resonances [46], and thus both quantities will provide additional control knobs. Finally, when going beyond a homogenous system, the nontrivial spatial BdG mode shapes $u_{\mathbf{q}}(\mathbf{x})$ and $v_{\mathbf{q}}(\mathbf{x})$ entering Eq. (18) will depend on the system geometry, for example, the trapping. A final interesting aspect would be the scaling in angular momentum $l, l+1$ of the two states involved in Fig. 5, where presently we fixed $l = 0, 1$.

We defer explorations of the above options to the future.

IV. CONCLUSIONS AND OUTLOOK

We have studied an immobile Rydberg excited atom within an atomic Bose-Einstein condensate, treating the latter as a controllable environment for the electronic states of the former. For this environment of phonon excitations in the BEC, we have introduced a framework for the calculation of bath-correlation functions, spectral densities, and reorganisation energies. These are important quantities for open quantum system approaches and contain all relevant information about the environmental influence on the systems dynamics. Knowledge of the reorganization energy or the bath correlation function at time zero already allows one to estimate the relevant timescales for decoherence and phonon-induced Rydberg state transitions. We found that they vary over orders of magnitude as a function of the principal quantum number ν.

For the example of ^{84}Sr atoms, we find that estimated decoherence timescales $T_{\text{decoh}} = 1/\sqrt{2C^{(zz)}(0)}$ between angular momentum states $|\nu s\rangle$ and $|\nu p\rangle$ range from $T_{\text{decoh}} = 20$ ns at a principal quantum number $\nu = 40$ to $T_{\text{decoh}} = 0.9$ μs at $\nu = 120$ in an exemplary BEC density of $\rho = 4.9 \times 10^{20}$ m^{-3}. We show in a companion article [27] that phonon-induced Rydberg state transitions between $|\nu s\rangle$ and $|\nu p\rangle$ are negligible on these timescales. Bath memory times change from around $T_{\text{m}} = 56$ μs at a principal quantum number $\nu = 40$ to $T_{\text{m}} = 660$ μs at $\nu = 120$. Since Rydberg dynamics is limited by lifetimes in a similar range, they would thus necessarily be placed in the non-Markovian regime where system dynamics happens on timescales faster or comparable to the memory time.

While the resultant open-quantum system is already strongly tuneable in its system-environment coupling by variation of the principal quantum number of the Rydberg atom, additional tunability might arise when extending the interaction model, for example, to long-range dressed interactions [53]. By affecting also the condensate atoms [72], dressing additionally modifies the dispersion relation (9) which will in turn modify the spectral properties of the BEC environment. Further control knobs would arise through the shape of the condensate wave function when moving from the homogenous condensate considered here to tightly trapped clouds of atoms.

The phonon environment can also affect the motional degrees of freedom of the Rydberg impurity, akin to Brownian motion, as has been considered for ground-state impurities in Refs. [8,37,73–80]. It would be of interest to generalize those results to Rydberg impurities with long-range interactions as discussed here. However, we expect the electronic decoherence times given above to typically be faster than any spatial diffusion. Alternatively, the impurity could be spatially trapped to suppress that effect.

In the present work, we have focused on the electronic decoherence dynamics of the Rydberg atom. One might now also be interested in the coherence and correlation properties of the ambient BEC. So far, schemes based on ground-state impurities have been investigated and it has been shown theoretically that one can obtain information on coherence and correlation properties [36,81,82] and also on the temperature [75,83] of the BEC. These schemes can now directly be adapted to the case of the Rydberg impurity studied in the present work, using the present results. It is possible that Rydberg impurities offer advantages over ground-state atoms for some of these purposes, due to their stronger coupling to the condensate.

ACKNOWLEDGMENTS

We gladly acknowledge fruitful discussions with Rick Mukherjee, Abhijit Pendse, and Shivakant Tiwari and thank the Science and Engineering Research Board (SERB), Department of Science and Technology (DST), New Delhi, India, for financial support under Research Project No. EMR/2016/005462. We further are grateful for financial support from the Max-Planck Society under the MPG-IISER partner group program. R.N. acknowledges UKIERI- UGC Thematic Partnership No. IND/CONT/G/16-17/73 UKIERI-UGC project and DST-SERB for a Swarnajayanti fellowship (File No. SB/SJF/2020-21/19). A.E. acknowledges

support from the Deutsche Forschungsgemeinschaft (DFG) via a Heisenberg fellowship (Grant No. EI 872/5-1).

APPENDIX A: GROUND-RYDBERG STATE INTERACTION HAMILTONIAN

As discussed in Sec. II C, the Hamiltonian for ground-state Rydberg-state interactions is

$$\hat{H}_{\rm int} = \sum_{\alpha,\beta} \int d^3\mathbf{x} \int d^3\mathbf{y} \times \hat{\Psi}_g^\dagger(\mathbf{x})\hat{\Psi}_\alpha^\dagger(\mathbf{y}) U^{g\alpha\beta g}(\mathbf{x}-\mathbf{y})\hat{\Psi}_\beta(\mathbf{y})\hat{\Psi}_g(\mathbf{x}), \quad \text{(A1)}$$

with $\hat{\Psi}_{g,\alpha,\beta}(\mathbf{x})$ field operators that destroy a ground-state atom or Rydberg atom in states $|\,\alpha\,\rangle, |\,\beta\,\rangle$ respectively, at position $\mathbf{x}$. Here α denotes a complete set of quantum numbers $\{\nu, l, m\}$, and similarly β groups $\{\nu', l', m'\}$. We now insert the potential $U^{g\alpha\beta g}(\mathbf{x}-\mathbf{y})$ from (14) into (A1) and then assume the BdG expansion (7) for the ground-state field operator. Additionally, using the Rydberg field operator (3) restricted to a single mode $\hat{\Psi}_\alpha(\mathbf{x}) \approx \varphi_0(\mathbf{x})\hat{a}^{(\alpha)}$, we obtain

$$\hat{H}_{\rm int} = g_0 \sum_{\alpha,\beta} \iint d^3\mathbf{x} d^3\mathbf{y} (\phi_0^*(\mathbf{x}) + \hat{\chi}^\dagger(\mathbf{x}))\varphi_0^*(\mathbf{y})\hat{a}_\alpha^\dagger \times \psi^{*(\alpha)}(\mathbf{x}-\mathbf{y})\psi^{(\beta)}(\mathbf{x}-\mathbf{y}) \times \varphi_0(\mathbf{y})\hat{a}_\beta^\dagger(\phi_0(\mathbf{x}) + \hat{\chi}(\mathbf{x})). \quad \text{(A2)}$$

So far, the single-mode $\varphi_0(\mathbf{x})$ could still be delocalized, e.g., a trap ground state. In the following, we assume a fixed location of the Rydberg core at the origin, so that $|\varphi_0(\mathbf{y})|^2 \approx \delta^{(3)}(\mathbf{y})$. Inserting the expansion (8) of the fluctuation operators into BdG modes, we then reach

$$\hat{H}_{\rm int} = g_0 \sum_{\alpha,\beta} \hat{a}^{\dagger(\alpha)}\hat{a}^{(\beta)} \int d^3\mathbf{x} \Big\{ |\phi_0(\mathbf{x})|^2 + \Big[\phi_0^*(\mathbf{x}) \sum_{\mathbf{q}} (u_{\mathbf{q}}(\mathbf{x})\hat{b}_{\mathbf{q}} - v_{\mathbf{q}}^*(\mathbf{x})\hat{b}_{\mathbf{q}}^\dagger) + \phi_0(\mathbf{x}) \sum_{\mathbf{q}} (u_{\mathbf{q}}^*(\mathbf{x})\hat{b}_{\mathbf{q}}^\dagger - v_{\mathbf{q}}(\mathbf{x})\hat{b}_{\mathbf{q}})\Big]\Big\} \times \psi^{*(\alpha)}(\mathbf{x})\psi^{(\beta)}(\mathbf{x}). \quad \text{(A3)}$$

As the next simplification, we consider a real condensate mean field, $\phi_0(x) = \phi_0^*(x)$, which excludes, for example, condensates with nontrivial velocity profile. It includes, however, the homogeneous static case treated here later and typical simple trapped cases. Since we shall deal with a single impurity, we can finally identify $\hat{a}^{\dagger(\alpha)}\hat{a}^{(\beta)}$ with $|\,\alpha\,\rangle\langle\,\beta\,|$ and cast (A3) into the form

$$\hat{H}_{\rm int} = \sum_{\alpha,\beta} |\,\alpha\,\rangle\langle\,\beta\,| \sum_{\mathbf{q}} \big[\kappa_{\mathbf{q}}^{(\alpha\beta)}\hat{b}_{\mathbf{q}} + \kappa_{\mathbf{q}}^{*(\alpha\beta)}\hat{b}_{\mathbf{q}}^\dagger + E^{(\alpha\beta)}\big], \quad \text{(A4)}$$

with

$$\kappa_{\mathbf{q}}^{(\alpha\beta)} = g_0 \int d^3\mathbf{x}\, \psi^{*(\alpha)}(\mathbf{x})\psi^{(\beta)}(\mathbf{x})\phi_0(\mathbf{x})(u_{\mathbf{q}}(\mathbf{x}) - v_{\mathbf{q}}(\mathbf{x})), \quad \text{(A5)}$$

$$E^{(\alpha\beta)} = g_0 \int d^3\mathbf{x}\, \psi^{*(\alpha)}(\mathbf{x})\psi^{(\beta)}(\mathbf{x})|\phi_0(\mathbf{x})|^2, \quad \text{(A6)}$$

which for a homogenous condensate $\phi_0(\mathbf{x}) = \sqrt{\rho}$ with density ρ reduce to the expressions given in (17) and (18).

APPENDIX B: CALCULATION OF COUPLING CONSTANTS

The expression for coupling constants $\kappa_{\mathbf{q}}^{(\alpha\beta)}$ in Eq. (A5) applies for a Rydberg atom in an arbitrary real condensate. We now consider the simpler homogeneous case, which should be a good approximation whenever the condensate density does not significantly vary on length scale of the Rydberg orbital radius $r_{\rm orb}$. In that case, the Bogoliubov modes take the simple plane-wave form

$$u_{\mathbf{q}}(\mathbf{x}) = \frac{\bar{u}_q}{\sqrt{\mathcal{V}}} e^{i\mathbf{q}\cdot\mathbf{x}}, \quad v_{\mathbf{q}}(\mathbf{x}) = \frac{\bar{v}_q}{\sqrt{\mathcal{V}}} e^{i\mathbf{q}\cdot\mathbf{x}}, \quad \text{(B1)}$$

using $q = |\mathbf{q}|$. Then, (A5) becomes

$$\kappa_{\mathbf{q}}^{(\alpha\beta)} = \frac{g_0\sqrt{\rho}}{\sqrt{\mathcal{V}}}(\bar{u}_q - \bar{v}_q) \int d^3\mathbf{x}\ \psi^{*(\alpha)}(\mathbf{x})\psi^{(\beta)}(\mathbf{x}) e^{i\mathbf{q}\cdot\mathbf{x}}. \quad \text{(B2)}$$

We thus see that coupling constants are related to the Fourier transform of spatial Rydberg electron probability densities, for $\alpha = \beta$, or of products of two wave functions, for $\alpha \neq \beta$. The prefactor $\bar{u}_q - \bar{v}_q \to 0$ for $q \leqslant \xi$ and approaches one for $q > \xi$, where ξ is the healing length.

At this stage, we expand the plane waves in terms of spherical harmonics Y_{lm}, according to

$$e^{i\mathbf{q}\cdot\mathbf{x}} = 4\pi \sum_{l_1=0}^{\infty} \sum_{m_1=-l_1}^{l_1} i^{l_1} j_{l_1}(qr)\, Y_{l_1 m_1}(\hat{\mathbf{q}})\, Y_{l_1 m_1}^*(\hat{\mathbf{x}}). \quad \text{(B3)}$$

Here $j_{l_1}(\mathrm{qr})$ are spherical Bessel functions of the first kind, $\hat{\mathbf{q}} = \mathbf{q}/|\mathbf{q}|$ is a unit vector along the wave vector of the phonon, and $\hat{\mathbf{x}} = \mathbf{x}/|\mathbf{x}|$, while $r = |\mathbf{x}|$ and $q = |\mathbf{q}|$.

1. Evaluation of angular integrals for general quantum states

As described before, the indices for electronic states α [β] are shorthand for quantum numbers (ν, l, m) [(ν', l', m')]. The corresponding electronic wave function in the Rydberg state of a hydrogen or alkali atom can be written as

$$\psi^{(\alpha)} \equiv \psi_{\nu lm} = \mathcal{N}_{\nu l}\, R_{\nu l}(r) Y_{lm}(\Theta, \Phi), \quad \text{(B4)}$$

with normalization constant $\mathcal{N}_{\nu l}$ and radial wave function $R_{\nu l}(r)$, while the angular wave functions are spherical harmonics $Y_{lm}(\Theta, \Phi)$ in terms of angular coordinates of the electron Θ and Φ. Note that we use capitalized angles for the coordinates of the electron and lowercase ones for the direction of the phonon wave vector $\mathbf{q}$. For hydrogen states that we use in the following, $\mathcal{N}_{\nu l} = \sqrt{(\frac{2}{\nu a_0})^3 \frac{(\nu-l-1)!}{2\nu[(\nu+l)!]}}$, with Bohr radius a_0. The radial wave function $R_{\nu l}(r)$ has the usual analytical form in terms of exponential times Laguerre polynomials. For multielectron alkali atoms, $R_{\nu l}(r)$ could, for example, be numerically found using the Numerov method [45].

From Eq. (B2), using (B3) and (B4), we then obtain

$$\kappa_{\mathbf{q}}^{\nu lm,\nu' l' m'} = \frac{g_0\sqrt{\rho}}{\sqrt{\mathcal{V}}}(\bar{u}_q - \bar{v}_q)\,\mathcal{N}_{\nu l}\,\mathcal{N}_{\nu' l'} \times \int_0^\infty dr\, r^2 R^*_{\nu l}(r) R_{\nu' l'}(r) \times \int_0^{2\pi} d\Phi \int_0^\pi d\Theta \sin(\Theta) \times Y^*_{lm}(\Theta,\Phi) Y_{l'm'}(\Theta,\Phi) \times 4\pi \sum_{l_1,m_1} i^{l_1} j_{l_1}(qr)\, Y_{l_1 m_1}(\hat{\mathbf{q}})\, Y^*_{l_1 m_1}(\Theta,\Phi). \quad \text{(B5)}$$

The integral over three spherical harmonics gives

$$\int_0^{2\pi} d\Phi \int_0^\pi d\Theta \sin(\Theta)\, Y^*_{lm}(\Theta,\Phi)\, Y_{l'm'}(\Theta,\Phi) Y^*_{l_1 m_1}(\Theta,\Phi) = (-1)^m (-1)^{m_1} \sqrt{\frac{(2l+1)(2l'+1)(2l_1+1)}{4\pi}} \times \begin{pmatrix} l & l' & l_1 \\ 0 & 0 & 0 \end{pmatrix} \begin{pmatrix} l & l' & l_1 \\ -m & m' & -m_1 \end{pmatrix}, \quad \text{(B6)}$$

where the last two terms in brackets are Wigner 3-j symbols. We can thus rewrite Eq. (B5) as

$$\kappa_{\mathbf{q}}^{\nu lm,\nu' l' m'} = \frac{g_0\sqrt{\rho}}{\sqrt{\mathcal{V}}}(\bar{u}_q - \bar{v}_q)\mathcal{N}_{\nu l}\mathcal{N}_{\nu' l'} \times \int_0^\infty dr\, r^2 R^*_{\nu,l}(r) R_{\nu',l'}(r) 4\pi \sum_{l_1} j_{l_1}(qr) \times \sum_{l_1,m_1} (i)^{l_1} \left[\sqrt{\frac{(2l+1)(2l'+1)(2l_1+1)}{4\pi}} \times \begin{pmatrix} l & l' & l_1 \\ 0 & 0 & 0 \end{pmatrix} \begin{pmatrix} l & l' & l_1 \\ -m & m' & -m_1 \end{pmatrix}\right] Y_{l_1 m_1}(\hat{\mathrm{q}}), \quad \text{(B7)}$$

which will be useful for a general choice of states. Among the experimentally most accessible choices, we now further evaluate (B7) for s ($l=0, m=0$) and p ($l=1, m=0$) states, within the same principal quantum number manifold $\nu = \nu'$.

2. Coupling constant for the Rydberg s state

For $\alpha = (\nu 00)$ and $\beta = (\nu 00)$, we shall use the shorthand $\kappa_{\mathbf{q}}^{\nu 00,\nu 00} = \kappa_{\mathbf{q}}^{(ss)}$ for coefficients in Eq. (B5). Inserting this choice of quantum numbers into (B7) gives

$$\kappa_{\mathbf{q}}^{(ss)} = \frac{g_0\sqrt{\rho}}{\sqrt{\mathcal{V}}}(\bar{u}_q - \bar{v}_q)| \left[\left(\frac{2}{\nu a_0}\right)^3 \frac{(\nu-1)!}{2\nu(\nu!)}\right] \times \int_0^\infty dr\, r^2 |R_{\nu 0}(r)|^2 4\pi \sum_{l_1 m_1} j_{l_1}(qr)(i)^{l_1} \times \left[\sqrt{\frac{(2l_1+1)}{4\pi}} \begin{pmatrix} 0 & 0 & l_1 \\ 0 & 0 & 0 \end{pmatrix} \begin{pmatrix} 0 & 0 & l_1 \\ 0 & 0 & -m_1 \end{pmatrix}\right] \times Y_{l_1 m_1}(\hat{\mathbf{q}}). \quad \text{(B8)}$$

The orthogonality properties encoded in the Wigner-3j symbol now leave only the $l_1 = 0, m_1 = 0$ term of the double sum, and hence

$$\kappa_{\mathbf{q}}^{(ss)} = \kappa_{\mathbf{q}}^{*(ss)} = \frac{g_0\sqrt{\rho}}{\sqrt{\mathcal{V}}}(\bar{u}_q - \bar{v}_q)\left[\left(\frac{2}{\nu a_0}\right)^3 \frac{(\nu-1)!}{2\nu(\nu!)}\right] \times \int_0^\infty dr\, \mathrm{r}^2 |R_{\nu 0}(\mathrm{r})|^2 j_0(qr), \quad \text{(B9)}$$

where we already inserted $Y_{00}(\hat{\mathbf{q}}) = 1/\sqrt{4\pi}$ and noted that $\kappa_{\mathbf{q}}^{(ss)}$ is manifestly real. The final evaluation of the radial matrix element is deferred to Appendix B 5.

3. Coupling constant for the Rydberg p state

Similarly, the starting point for $\kappa_{\mathbf{q}}^{(pp)}$ will be

$$\kappa_{\mathbf{q}}^{(pp)} = \frac{g_0\sqrt{\rho}}{\sqrt{\mathcal{V}}}(\bar{u}_q - \bar{v}_q)| \left[\left(\frac{2}{\nu a_0}\right)^3 \frac{(\nu-2)!}{2\nu[(\nu+1)!]}\right] \times \int_0^\infty dr\, r^2 |R_{\nu 1}(r)|^2 4\pi \sum_{l_1,m_1} j_{l_1}(qr)(i)^{l_1} \times \left[\sqrt{\frac{9\,(2l_1+1)}{4\pi}} \begin{pmatrix} 1 & 1 & l_1 \\ 0 & 0 & 0 \end{pmatrix} \begin{pmatrix} 1 & 1 & l_1 \\ 0 & 0 & -m_1 \end{pmatrix}\right] \times Y_{l_1 m_1}(\hat{\mathrm{q}}). \quad \text{(B10)}$$

As in case of $\kappa_{\mathbf{q}}^{(ss)}$, the selection rules in the Wigner symbols help us to restrict the summation for $\kappa_{\mathbf{q}}^{(pp)}$ in Eq. (B10) to obtain

$$\kappa_{\mathbf{q}}^{(pp)} = \kappa_{\mathbf{q}}^{*(pp)} = \frac{g_0\sqrt{\rho}}{\sqrt{\mathcal{V}}}(u_{\mathbf{q}} - v_{\mathbf{q}})| \left[\left(\frac{2}{\nu a_0}\right)^3 \frac{(\nu-2)!}{2\nu[(\nu+1)!]}\right] \times 3\sqrt{4\pi}\left[\frac{1}{3}Y_{00}(\hat{\mathrm{q}}) \int_0^\infty dr\, r^2 |R_{\nu 1}(r)|^2 j_0(qr) - \frac{2\sqrt{5}}{15} Y_{20}(\hat{\mathrm{q}}) \int_0^\infty dr\, r^2 |R_{\nu 1}(r)|^2 j_2(qr)\right], \quad \text{(B11)}$$

which is again manifestly real.

4. Coupling constant for sp

Finally, we follow the same procedure for the coupling constant $\kappa_{\mathbf{q}}^{(sp)}$ and find

$$\kappa_{\mathbf{q}}^{(sp)} = -\kappa_{\mathbf{q}}^{*(sp)} = i\,\frac{g_0\sqrt{\rho}}{\sqrt{\mathcal{V}}}(\bar{u}_{\mathrm{q}} - \bar{v}_{\mathrm{q}}) \sqrt{\left(\frac{2}{\nu a_0}\right)^3 \frac{(\nu-1)!}{2\nu(\nu!)}} \times \sqrt{\left(\frac{2}{\nu a}\right)^3 \frac{(\nu-2)!}{2\nu[(\nu+1)!]}} \int_0^\infty dr\, r^2 R^*_0(r) \times R_1(\mathrm{r})\, j_1(qr) Y_{10}(\hat{\mathrm{q}}). \quad \text{(B12)}$$

In contrast to the expressions in the two subsections before, this coupling is fully imaginary as indicated.

5. Evaluation of radial matrix elements

To reach explicit forms for (B9), (B11), and (B12), we have to evaluate the remaining radial matrix elements.

TABLE I. Parameters in fit functions (B16)–(B18) for Rydberg-phonon coupling coefficients κ. Physical parameters are as for Fig. 2.

Function	A $\left[\frac{\mathrm{s}}{\mathrm{kg\ m^{7/2}}}\right]$	α_1 [μm]	β_1	γ_1 [μm]	B $\left[\frac{\mathrm{s}}{\mathrm{kg\ m^{7/2}}}\right]$	α_2 [μm]	β_2	γ_2 [μm]
$f^{(ss)}$	2.28×10^{45}	0.002	0.002	0.13	-6.82×10^{42}	0.16	1.48	0.025
$f_1^{(pp)}$	2.19×10^{45}	0.002	0.002	0.135	-6.83×10^{42}	0.16	1.48	0.026
$f_2^{(pp)}$	0.54×10^{45}	−0.002	−3.15	0.07	-5.84×10^{42}	0.15	−1.02	0.024
$f^{(sp)}$	6.94×10^{42}	0	−0.98	0.04	-5.75×10^{42}	0.15	−2.95	0.037

a. Involving Rydberg s states

For $\kappa_{\mathbf{q}}^{(ss)}$, this is possible analytically. From Eq. (B2), we can write

$$\kappa_{\mathbf{q}}^{(ss)} = \frac{g_0\sqrt{\rho}}{\sqrt{\mathcal{V}}}(\bar{u}_q - \bar{v}_q)\int d^3\mathbf{x}\ |\psi^{(s)}(\mathbf{x})|^2 e^{i\mathbf{q}\cdot\mathbf{x}}. \tag{B13}$$

When we expand the integration using three-dimensional (3D) spherical coordinates defined earlier, the radial part involves an integration over exponential functions times Laguerre polynomials, which has an explicit solution [84]. The final coupling constant then takes the form

$$\begin{aligned}\kappa_q^{(ss)} = \frac{g_0\sqrt{\rho}}{\sqrt{\mathcal{V}}}(\bar{u}_q - \bar{v}_q) \times \frac{i\,\mathcal{N}_{\nu 0}^2}{2q} \times \frac{\Gamma(2\nu)(iq)^{2(\nu-1)}}{(\nu-1)!^2} \\ \times \left[\frac{1}{\left[\left(\frac{2}{\nu a_0}\right) - iq\right]^{2\nu}} - \frac{1}{\left[\left(\frac{2}{\nu a_0}\right) + iq\right]^{2\nu}}\right] \\ \times {}_2F_1\left[1-\nu, 1-\nu; 1-2\nu, 1+\left(\frac{2}{\nu a_0 q}\right)^2\right],\end{aligned} \tag{B14}$$

where ${}_2F_1$ denotes the Gauss hypergeometric function and Γ is the Gamma function.

b. Involving Rydberg p states

Although analytic expressions exist also for radial integrations involving p states in (B11) and (B12) [85], these are quite involved and we hence opted to perform those integrations numerically, which will also allow the future incorporation of numerically determined wave functions for alkali atoms. Since we later have to evaluate further integrations over the coupling constant as a function of momenta $\mathbf{q}$, it is beneficial to fit the results of the radial numerical integration with a simple functional form, which we describe now. While the coefficient $\kappa_q^{(ss)}$ does have an analytical expression in (B14), we found it convenient to treat all coupling on the same footing and also proceed with $\kappa_q^{(ss)}$ using the fitting procedure.

To this end, we define a function template

$$T(q) = A\sin(\alpha_1 q + \beta_1)e^{-\gamma_1 q} + B\cos(\alpha_2 q + \beta_2)e^{-\gamma_2 q}, \tag{B15}$$

and then express

$$\sqrt{\mathcal{V}}\kappa_{\mathbf{q}}^{(ss)}/g_0 = f^{(ss)}(q), \tag{B16}$$

$$\sqrt{\mathcal{V}}\kappa_{\mathbf{q}}^{(sp)}/g_0 = f^{(sp)}(q)\cos(\theta), \tag{B17}$$

$$\sqrt{\mathcal{V}}\kappa_{\mathbf{q}}^{(pp)}/g_0 = f_1^{(pp)}(q) - f_2^{(pp)}(q)[3\cos^2(\theta) - 1], \tag{B18}$$

where each of the functions $f^{(ss)}(q)$, $f^{(sp)}(q)$, $f_1^{(pp)}(q)$, $f_2^{(pp)}(q)$ has the form of the template $T(q)$, with different coefficients $A, B, \alpha_1, \beta_1, \gamma_1, \alpha_2, \beta_2$, and γ_2 as listed in Table I. We have excluded $\sqrt{\mathcal{V}}$ from the fit since the quantization volume must cancel in the calculation of physical quantities later and g_0 to facilitate the conversion of the results to other atomic species. The quality of these fits is shown in Fig. 6.

6. Formulation of the final Hamiltonian

Now that all coupling constants that enter the interaction Hamiltonian Eq. (A4) in the Rydberg manifolds $|\,\nu, l=0\,\rangle$ and $|\,\nu, l=1\,\rangle$ are known, via (B9), (B11), and (B12), we proceed to regroup that Hamiltonian. Note that all terms $E^{(\alpha\beta)}$ with $\alpha, \beta \in \{s, p\}$ do not contain BdG mode operators, and hence will be reallocated to the system Hamiltonian. Using the identification $|\uparrow\rangle = |\,p\,\rangle$ and $|\downarrow\rangle = |\,s\,\rangle$ discussed in Sec. III and Pauli spin matrices, we rewrite the remaining terms as

$$\begin{aligned}\hat{H}_{\mathrm{int}} = &\sum_{\mathbf{q}} \frac{\left(\kappa_{\mathbf{q}}^{(pp)} - \kappa_{\mathbf{q}}^{(ss)}\right)}{2}(\hat{b}_{\mathbf{q}} + \hat{b}_{\mathbf{q}}^\dagger)\hat{\sigma}_z \\ &+ \sum_{\mathbf{q}} \frac{\left(\kappa_{\mathbf{q}}^{(pp)} + \kappa_{\mathbf{q}}^{(ss)}\right)}{2}(\hat{b}_{\mathbf{q}} + \hat{b}_{\mathbf{q}}^\dagger)\mathbb{1} \\ &+ i\sum_{\mathbf{q}} \kappa_{\mathbf{q}}^{(sp)}(\hat{b}_{\mathbf{q}} - \hat{b}_{\mathbf{q}}^\dagger)\hat{\sigma}_y,\end{aligned} \tag{B19}$$

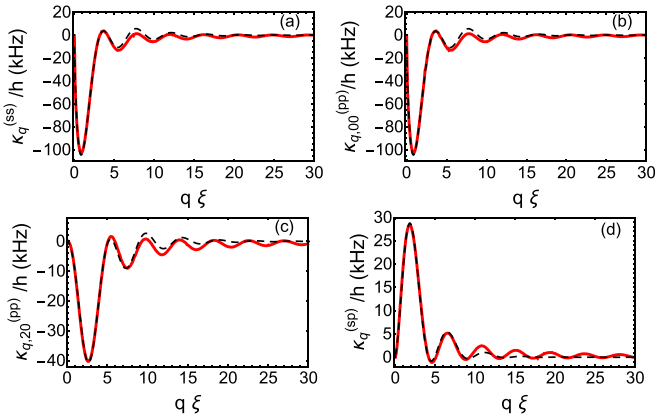

FIG. 6. (a) Coupling constant $\kappa_q^{(ss)}$ (red solid) of state $|\,s\,\rangle$ to a phonon with wave number q for principal quantum number $\nu = 40$ as in Fig. 2 and the fit (black dashed) $g_0 f^{(ss)}/\sqrt{\mathcal{V}}$ from (B16) with the parameters in Table I. (b) Isotropic part of the coupling constant $\kappa_{q,00}^{(pp)}$ of state $|\,p\,\rangle$ with its the fit $g_0 f_1^{(pp)}/\sqrt{\mathcal{V}}$ and (c) the anisotropic part $\kappa_{q,20}^{(pp)}$ with the fit $g_0 f_2^{(pp)}/\sqrt{\mathcal{V}}$ from (B18). (d) The transition coupling $\kappa_q^{(sp)}$ between $|\,s\,\rangle$ and $|\,p\,\rangle$ to a phonon with wave number q and its fit $g_0 f^{(sp)}/\sqrt{\mathcal{V}}$ from (B17).

where $\mathbb{1}$ is the unit operator in the Rydberg electronic state space. Let us define $\bar{\kappa}_{\mathbf{q}} = \kappa_{\mathbf{q}}^{(pp)} + \kappa_{\mathbf{q}}^{(ss)}$ and $\Delta\kappa_{\mathbf{q}} = \kappa_{\mathbf{q}}^{(pp)} - \kappa_{\mathbf{q}}^{(ss)}$ and then consider jointly the present interaction Hamiltonian and the environmental Hamiltonian from (10):

$$\hat{H}_{\rm env} + \hat{H}_{\rm int} = E_{GP} + \sum_{\mathbf{q}} \hbar\omega_{\mathbf{q}} \hat{b}_{\mathbf{q}}^{\dagger}\hat{b}_{\mathbf{q}} + \sum_{\mathbf{q}} \frac{\Delta\kappa_{\mathbf{q}}}{2}(\hat{b}_{\mathbf{q}} + \hat{b}_{\mathbf{q}}^{\dagger})\hat{\sigma}_z + \sum_{\mathbf{q}} \frac{\bar{\kappa}_{\mathbf{q}}}{2}(\hat{b}_{\mathbf{q}} + \hat{b}_{\mathbf{q}}^{\dagger})\mathbb{1} + i\sum_{\mathbf{q}} \kappa_{\mathbf{q}}^{(sp)}(\hat{b}_{\mathbf{q}} - \hat{b}_{\mathbf{q}}^{\dagger})\hat{\sigma}_y. \tag{B20}$$

We can then absorb the term $\sim\mathbb{1}$ by using shifted environmental mode operators

$$\tilde{b}_{\mathbf{q}} = \hat{b}_{\mathbf{q}} + \frac{\bar{\kappa}_{\mathbf{q}}}{2\hbar\omega_q}, \tag{B21}$$

$$\tilde{b}_{\mathbf{q}}^{\dagger} = \hat{b}_{\mathbf{q}}^{\dagger} + \frac{\bar{\kappa}_{\mathbf{q}}^{*}}{2\hbar\omega_q}. \tag{B22}$$

We use these in the Hamiltonian (B20) and then allocate all terms that do not contain environmental operators $\tilde{b}_{\mathbf{q}}$ or $\tilde{b}_{\mathbf{q}}^{\dagger}$ to a shifted system Hamiltonian, so that our final result for the complete Hamiltonian $\hat{H} = \hat{H}'_{\rm syst} + \hat{H}_{\rm coup} + \hat{H}'_{\rm env} + \text{const.}$ becomes

$$\hat{H}'_{\rm syst} = \hat{H}_{\rm syst} - \sum_{\mathbf{q}} \frac{\Delta\kappa_{\mathbf{q}}\bar{\kappa}_{\mathbf{q}}}{2\hbar\omega_q}\hat{\sigma}_z, \tag{B23a}$$

$$\hat{H}'_{\rm env} = \sum_{\mathbf{q}} \hbar\omega_q\, \tilde{b}_{\mathbf{q}}^{\dagger}\tilde{b}_{\mathbf{q}}, \tag{B23b}$$

$$\hat{H}_{\rm coup} = \sum_{\mathbf{q}} \frac{\Delta\kappa_{\mathbf{q}}}{2}(\tilde{b}_{\mathbf{q}} + \tilde{b}_{\mathbf{q}}^{\dagger})\hat{\sigma}_z + i\sum_{\mathbf{q}} \kappa_{\mathbf{q}}^{(sp)}(\tilde{b}_{\mathbf{q}} - \tilde{b}_{\mathbf{q}}^{\dagger})\hat{\sigma}_y, \tag{B23c}$$

where the constant energy offset in $\hat{H}$ has absorbed some contributions from (B20).

We can evaluate the environment induced energy shift in H'_{syst} after converting the discrete summation over modes to a continuous integral, $\sum_{\mathbf{q}} \longrightarrow \int d^3\mathbf{q} D$, with density of states $D = \mathcal{V}/(2\pi)^3$, and find

$$\bar{E}\hat{\sigma}_z \equiv -\sum_{\mathbf{q}} \frac{\Delta\kappa_{\mathbf{q}}\bar{\kappa}_{\mathbf{q}}}{2\hbar\omega_q}\hat{\sigma}_z = D\int d^3\mathbf{q}\frac{\Delta\kappa_{\mathbf{q}}\bar{\kappa}_{\mathbf{q}}}{2\hbar\omega_q\mathcal{V}}\hat{\sigma}_z = 2\pi D\int_0^{\infty} dq\, q^2\left[\frac{2f_1^{(pp)}(q)^2 + \frac{8}{5}f_2^{(pp)}(q)^2 - 2f^{(ss)}(q)^2}{2\hbar\omega_q}\right]\hat{\sigma}_z, \tag{B24}$$

where we already integrated over θ and φ. Evaluating the final integral, we reach, for example, $\bar{E} = 1.7$ GHz using the parameters of Fig. 2. For later use, we finally split $\hat{H}_{\rm coup} = \hat{\sigma}_z \otimes \hat{E}^{(z)} + \hat{\sigma}_y \otimes \hat{E}^{(y)}$, with

$$\hat{E}^{(z)} = \sum_{\mathbf{q}} \frac{\kappa_{\mathbf{q}}^{(pp)} - \kappa_{\mathbf{q}}^{(ss)}}{2}[\tilde{b}_{\mathbf{q}} + \tilde{b}_{\mathbf{q}}^{\dagger}], \tag{B25}$$

$$\hat{E}^{(y)} = i\sum_{\mathbf{q}} \kappa_{\mathbf{q}}^{(sp)}[\tilde{b}_{\mathbf{q}} - \tilde{b}_{\mathbf{q}}^{\dagger}]. \tag{B26}$$

A very important final point is that after redefining the BdG operators as in (B21), they fulfill

$$\tilde{b}_{\mathbf{q}}|\,0\,\rangle = d_{\mathbf{q}}|\,0\,\rangle, \tag{B27}$$

$$\langle\,0\,|\tilde{b}_{\mathbf{q}}^{\dagger} = \langle\,0\,|d_{\mathbf{q}}^{*}, \tag{B28}$$

for $d_{\mathbf{q}} = \frac{\bar{\kappa}_{\mathbf{q}}}{2\hbar\omega_q}$, where $|\,0\,\rangle$ is the BdG vacuum for the original unshifted operators $\hat{b}$. These equations make clear that in terms of the new operators the original BdG vacuum is a many-mode coherent state or *displaced* vacuum. However, we will show in the next section that open quantum system dynamics with an environment initialised in a coherent state is equivalent to one with an environment in a vacuum state and a slight shift in the Hamiltonian. Hence, we subsequently consider also the environment state $\hat{\rho}_{\mathcal{E}}$ for the newly defined operators $\tilde{b}_{\mathbf{q}}$ to be the vacuum state.

APPENDIX C: TRANSFORMATION OF ENVIRONMENTAL STATE

We had seen in the preceding Appendix that in order to reach a standard form of the spin-boson model in (B23), it has to be formulated in terms of Bogoliubov operators shifted as in Eq. (B21). Thus, the initial environment vacuum state $\hat{\rho}_{\mathcal{E}} = |\,0\,\rangle\langle\,0\,|$ for operators $\hat{b}_{\mathbf{q}}$ becomes $\hat{\rho}_{\mathcal{E}} = |\,\mathbf{d}\,\rangle\langle\,\mathbf{d}\,|$, where $|\,\mathbf{d}\,\rangle$ is a many-mode coherent state of the environment. This implies that for each operator $\tilde{b}_{\mathbf{q}}$, it acts as a coherent state with amplitude $d_{\mathbf{q}}$.

Let us insert this state into (19), and then rewrite the many-mode coherent state using the standard displacement operator $|\,\mathbf{d}\,\rangle = \hat{D}(\mathbf{d})|\,0\,\rangle$, where $\hat{D}(\mathbf{d}) = \prod_{\mathbf{q}} \exp(d_{\mathbf{q}}\tilde{b}_{\mathbf{q}}^{\dagger} - d_{\mathbf{q}}^{*}\tilde{b}_{\mathbf{q}})$. We find

$$\begin{aligned}\hat{\rho}_{\mathcal{S}}(t) &= \mathrm{Tr}_{\mathcal{E}}(\hat{U}(t)[\hat{\rho}_{\mathcal{S}}(0)\otimes|\,\mathbf{d}\,\rangle\langle\,\mathbf{d}\,|]\hat{U}^{\dagger}(t)) \\ &= \mathrm{Tr}_{\mathcal{E}}(\hat{U}(t)[\hat{\rho}_{\mathcal{S}}(0)\otimes\hat{D}(\mathbf{d})|\,0\,\rangle\langle\,0\,|\hat{D}^{\dagger}(\mathbf{d})] \\ &\quad\times\hat{U}^{\dagger}(t)\hat{D}(\mathbf{d})\hat{D}^{\dagger}(\mathbf{d})),\end{aligned} \tag{C1}$$

where we have also inserted $\mathbb{1} = \hat{D}(\mathbf{d})\hat{D}^{\dagger}(\mathbf{d})$ into the trace.

This can be rearranged into

$$\hat{\rho}_{\mathcal{S}}(t) = \mathrm{Tr}_{\mathcal{E}}(\tilde{U}(t)[\hat{\rho}_{\mathcal{S}}(0)\otimes|\,0\,\rangle\langle\,0\,|]\tilde{U}^{\dagger}(t)), \tag{C2}$$

where the time evolution is now governed by the shifted time evolution operator $\tilde{U}(t) = \hat{D}(\mathbf{d})\hat{U}(t)\hat{D}^{\dagger}(\mathbf{d})$, but starts from a vacuum environment initial state. That time evolution operator arises in turn from a shifted Hamiltonian $\tilde{H} =$

$\hat{D}(\mathbf{d})\hat{H}(t)\hat{D}^{\dagger}(\mathbf{d})$, where $\hat{H}(t)$ is the interaction picture Hamiltonian following from (B23).

This shifted Hamiltonian finally takes the form

$$\hat{H}''_{\rm syst} = \hat{H}'_{\rm syst} + \hat{\sigma}_z \sum_{\mathbf{q}} \frac{\Delta\kappa_{\mathbf{q}}\,\bar{\kappa}_{\mathbf{q}}}{2\hbar\omega_q}\cos(\omega_q t), \tag{C3}$$

where $\hat{H}'_{\rm syst}$ was given in Eq. (B23). We shall explore the ramifications of this term for our scenario in Ref. [27]. A similar procedure was used in Ref. [86] to handle finite-temperature environments.

APPENDIX D: CALCULATION OF BEC ENVIRONMENT CORRELATION FUNCTIONS

As discussed in Sec. III A, the effect of the BEC environment on the Rydberg impurity is fully encapsulated in the environmental correlation functions defined in Eq. (28). These equations define three different correlation functions, owing to the two nontrivial parts of the system-environment coupling Hamiltonian (B23). Correlations depend on the assumed state of the environment, for which we can take the vacuum state as shown in Appendix C.

1. *zz* correlations

Inserting Eq. (B25) into $C^{(zz)}(\tau)$ of Eq. (28), we can write

$$C^{(zz)}(\tau) = \sum_{\mathbf{q},\mathbf{q}'} \frac{\Delta\kappa_{\mathbf{q}}}{2}\frac{\Delta\kappa_{\mathbf{q}'}}{2} \times \langle 0\,|[\tilde{b}_{\mathbf{q}}(\tau) + \tilde{b}^{\dagger}_{\mathbf{q}}(\tau)][\tilde{b}_{\mathbf{q}'}(0) + \tilde{b}^{\dagger}_{\mathbf{q}'}(0)]|\,0\rangle. \tag{D1}$$

In the interaction picture, we have

$$\tilde{b}_{\mathbf{q}}(\tau) = \tilde{b}_{\mathbf{q}}(0)e^{-i\omega_q\tau}, \tag{D2}$$

$$\tilde{b}^{\dagger}_{\mathbf{q}}(\tau) = \tilde{b}^{\dagger}_{\mathbf{q}}(0)e^{i\omega_q\tau}. \tag{D3}$$

Hence Eq. (D1) becomes

$$C^{(zz)}(\tau) = \sum_{\mathbf{q}} \frac{\Delta\kappa^2_{\mathbf{q}}}{4}e^{-i\omega_q\tau}. \tag{D4}$$

To evaluate (D4), we again convert from the discrete to a continuous notation, according to $\sum_{\mathbf{q}} \longrightarrow \int d^3\mathbf{q}\, D$. As expected, we see that the quantization volume $\mathcal{V}$ from the $\sum_{\mathbf{q}}$ cancels those from $\Delta\kappa_{\mathbf{q}}$ and $d_{\mathbf{q}}$; see, e.g., Eq. (B9). Let us denote the 3D spherical coordinates of the wave vector $\mathbf{q}$ with $q = |\mathbf{q}|$, θ, and φ. We now insert the fitted coupling constants obtained in Appendix B 5 to obtain

$$d_{\mathbf{q}} = \frac{g_0}{\sqrt{\mathcal{V}}}\frac{f_1^{(pp)}(q) - f_2^{(pp)}(q)[3\cos^2(\theta)-1] + f^{(ss)}(q)}{2\hbar\omega_q}, \tag{D5}$$

$$\Delta\kappa_{\mathbf{q}} = \frac{g_0}{\sqrt{\mathcal{V}}}\left\{f_1^{(pp)}(q) - f_2^{(pp)}(q)[3\cos^2(\theta)-1] - f^{(ss)}(q)\right\}. \tag{D6}$$

Evaluating angular integrals, we find

$$C^{(zz)}(\tau) = \pi g_0^2 D\int_0^{\infty} dq\, q^2 e^{-i\omega_{\mathbf{q}}\tau} \times \left[f_1^{(pp)}(q)^2 + \frac{4}{5}f_2^{(pp)}(q)^2 + f^{(ss)}(q)^2 - 2f_1^{(pp)}(q)f^{(ss)}(q)\right], \tag{D7}$$

after also integrating over the azimuthal angle φ. The integrations over q are finally performed numerically, with results shown in Fig. 3.

2. *yy* correlations

The calculation of environmental correlation functions involving the operator $\hat{E}^{(yy)}$ proceeds similarly. After insertion of interaction picture bath operators, we now have

$$C^{(yy)}(\tau) = \sum_{\mathbf{q}}\left[\kappa^{(sp)}_{\mathbf{q}}\right]^2\langle 0\,|\tilde{b}_{\mathbf{q}}(0)e^{-i\omega_{\mathbf{q}}\tau}\tilde{b}^{\dagger}_{\mathbf{q}}(0)|\,0\rangle. \tag{D8}$$

After the same conversion from discrete to continuous bath modes as in the previous section, we reach

$$C^{(yy)}(\tau) = -\frac{4\pi}{3}g_0^2 D\int_0^{\infty} dq\, q^2 f^{(sp)}(q)^2 e^{-i\omega_q\tau}. \tag{D9}$$

3. *yz* correlations

For a system environment Hamiltonian containing two coupling terms such as (B23), in principle also cross-correlation functions between environmental operators in those two terms may become relevant. However, we show now that

$$C^{(zy)}(\tau) = \langle 0\,|\hat{E}^{(z)}(\tau)\hat{E}^{(y)}(0)|\,0\rangle \tag{D10}$$

vanishes in our case. As before, we insert (B25) and (B26) into (D10) to find

$$C^{(zy)}(\tau) = -i\sum_{\mathbf{q}}\frac{\Delta\kappa_{\mathbf{q}}}{2}\kappa^{(sp)}_{\mathbf{q}}e^{-i\omega_{\mathbf{q}}\tau}. \tag{D11}$$

The angular structure of the resultant integral is odd and the integral vanishes, so that $C^{(zy)}(\tau) = 0$.

APPENDIX E: CALCULATION OF SPECTRAL DENSITIES

As discussed in Sec. III B, spectral densities contain interesting information on environmental properties. We can obtain them directly from the definition (30)

$$J^{(z)}(\omega) = \sum_{\mathbf{q}}\frac{\Delta\kappa^2_{\mathbf{q}}}{4}\delta(\omega - \omega_{\mathbf{q}}). \tag{E1}$$

If we convert the sum to a continuum integral, we can write this as

$$J^{(z)}(\omega) = \int_0^{\infty} d^3\mathbf{q}\,\frac{\Delta\kappa^2_{\mathbf{q}}}{4}\delta(\omega - \omega_{\mathbf{q}})D, \tag{E2}$$

where $\omega_{\mathbf{q}} = \sqrt{\frac{\hbar q^2}{2m}\left(\frac{\hbar^2 q^2}{2m} + 2U_0\rho\right)}$. To evaluate the delta function, we require

$$\frac{d\omega_q}{dq} = \frac{\frac{\hbar^2 q^2}{m^2} + \frac{2U_0\rho}{m}}{2\sqrt{\frac{\hbar^2 q^2}{4m^2} + \frac{U_0\rho}{m}}} \tag{E3}$$

and using the parametrizations (B16) and (B18) for $\Delta\kappa_{\mathbf{q}}$ we finally reach

$$J^{(z)}(\omega) = \frac{\pi D}{\sqrt{2}} q_\omega^2 \Big[f_1^{(pp)}(q_\omega)^2 + \frac{4}{5} f^{(ss)}(q_\omega)^2 + f^{(sp)}(q_\omega)^2 - 2 f_1^{(pp)}(q_\omega) f^{(ss)}(q_\omega) \Big] \frac{dq_\omega}{d\omega_q}, \quad \text{(E4)}$$

with $q_\omega = \frac{\sqrt{2m}}{\hbar} \sqrt{\sqrt{(\hbar\omega)^2 + (U_0\rho)^2} - U_0\rho}$.

Similarly the spectral density for the $\hat{\sigma}_y$ coupling can be written as

$$J^{(y)}(\omega) = \int_0^\infty d^3\mathbf{q}\, \kappa_{\mathbf{q}}^{(sp)\,2} \delta(\omega - \omega_{\mathbf{q}}) D, \quad \text{(E5)}$$

which will have the final form

$$J^{(y)}(\omega) = \frac{\pi D}{\sqrt{2}} q_\omega^2 \left[\frac{1}{3} f^{(sp)}(q_\omega)^2 \right] \frac{dq_\omega}{d\omega_q}. \quad \text{(E6)}$$

We explicitly verified that the same spectral densities are obtained via the Fourier transform relation (32).

[1] C. Zipkes, S. Palzer, C. Sias, and M. Köhl, Nature (London) **464**, 388 (2010).
[2] S. Schmid, A. Härter, and J. H. Denschlag, Phys. Rev. Lett. **105**, 133202 (2010).
[3] K. S. Kleinbach, F. Engel, T. Dieterle, R. Löw, T. Pfau, and F. Meinert, Phys. Rev. Lett. **120**, 193401 (2018).
[4] S. Dutta and S. A. Rangwala, Phys. Rev. A **97**, 041401(R) (2018).
[5] T. Dieterle, M. Berngruber, C. Hölzl, R. Löw, K. Jachymski, T. Pfau, and F. Meinert, Phys. Rev. A **102**, 041301(R) (2020).
[6] N. Spethmann, F. Kindermann, S. John, C. Weber, D. Meschede, and A. Widera, Phys. Rev. Lett. **109**, 235301 (2012).
[7] R. Wynar, R. Freeland, D. Han, C. Ryu, and D. Heinzen, Science **287**, 1016 (2000).
[8] A. Klein, M. Bruderer, S. R. Clark, and D. Jaksch, New J. Phys. **9**, 411 (2007).
[9] T. H. Johnson, S. R. Clark, M. Bruderer, and D. Jaksch, Phys. Rev. A **84**, 023617 (2011).
[10] M. Cetina, M. Jag, R. S. Lous, I. Fritsche, J. T. Walraven, R. Grimm, J. Levinsen, M. M. Parish, R. Schmidt, M. Knap *et al.*, Science **354**, 96 (2016).
[11] A. Schirotzek, C.-H. Wu, A. Sommer, and M. W. Zwierlein, Phys. Rev. Lett. **102**, 230402 (2009).
[12] A. C. Hewson, *The Kondo Problem to Heavy Fermions* (Cambridge University Press, Cambridge, UK, 1997).
[13] M. Nakagawa, N. Kawakami, and M. Ueda, Phys. Rev. Lett. **121**, 203001 (2018).
[14] F. Grusdt, R. Schmidt, Y. E. Shchadilova, and E. Demler, Phys. Rev. A **96**, 013607 (2017).
[15] F. Camargo, R. Schmidt, J. D. Whalen, R. Ding, G. Woehl, S. Yoshida, J. Burgdörfer, F. B. Dunning, H. R. Sadeghpour, E. Demler, and T. C. Killian, Phys. Rev. Lett. **120**, 083401 (2018).
[16] R. Schmidt, J. D. Whalen, R. Ding, F. Camargo, G. Woehl, S. Yoshida, J. Burgdörfer, F. B. Dunning, E. Demler, H. R. Sadeghpour, and T. C. Killian, Phys. Rev. A **97**, 022707 (2018).
[17] M. Bruderer, A. Klein, S. R. Clark, and D. Jaksch, Phys. Rev. A **76**, 011605(R) (2007).
[18] M. Bruderer, A. Klein, S. R. Clark, and D. Jaksch, New J. Phys. **10**, 033015 (2008).
[19] M. Knap, A. Shashi, Y. Nishida, A. Imambekov, D. A. Abanin, and E. Demler, Phys. Rev. X **2**, 041020 (2012).
[20] R. Heidemann, U. Raitzsch, V. Bendkowsky, B. Butscher, R. Löw, and T. Pfau, Phys. Rev. Lett. **100**, 033601 (2008).
[21] J. B. Balewski, A. T. Krupp, A. Gaj, D. Peter, H. P. Büchler, R. Löw, S. Hofferberth, and T. Pfau, Nature (London) **502**, 664 (2013).
[22] A. Gaj, A. T. Krupp, J. B. Balewski, R. Löw, S. Hofferberth, and T. Pfau, Nat. Commun. **5**, 4546 (2014).
[23] M. Schlagmüller, T. C. Liebisch, H. Nguyen, G. Lochead, F. Engel, F. Böttcher, K. M. Westphal, K. S. Kleinbach, R. Löw, S. Hofferberth *et al.*, Phys. Rev. Lett. **116**, 053001 (2016).
[24] I. Beterov and P. Lerner, Sov. Phys. Uspekhi **32**, 1084 (1989).
[25] R. Löw, H. Weimer, J. Nipper, J. B. Balewski, B. Butscher, H. P. Büchler, and T. Pfau, J. Phys. B **45**, 113001 (2012).
[26] S. K. Saikin, A. Eisfeld, S. Valleau, and A. Aspuru-Guzik, Nanophotonics **2**, 21 (2013).
[27] S. Rammohan, S. Tiwari, A. Mishra, A. Pendse, A. Kumar, R. Nath, A. Eisfeld, and S. Wüster, arXiv:2011.11022.
[28] D. W. Schönleber, A. Eisfeld, M. Genkin, S. Whitlock, and S. Wüster, Phys. Rev. Lett. **114**, 123005 (2015).
[29] H. Schempp, G. Günter, S. Wüster, M. Weidemüller, and S. Whitlock, Phys. Rev. Lett. **115**, 093002 (2015).
[30] F. Schmidt, D. Mayer, Q. Bouton, D. Adam, T. Lausch, N. Spethmann, and A. Widera, Phys. Rev. Lett. **121**, 130403 (2018).
[31] F. Schmidt, D. Mayer, T. Lausch, D. Adam, Q. Bouton, M. Hohmann, F. Kindermann, J. Koch, J. Nettersheim, and A. Widera, Phys. Stat. Solidi B **256**, 1800710 (2019).
[32] Y.-J. Song and L.-M. Kuang, Ann. Phys. **531**, 1800423 (2019).
[33] P. Ostmann and W. T. Strunz, arXiv:1707.05257.
[34] S. McEndoo, P. Haikka, G. De Chiara, G. Palma, and S. Maniscalco, EPL **101**, 60005 (2013).
[35] M. Cirone, G. De Chiara, G. Palma, and A. Recati, New J. Phys. **11**, 103055 (2009).
[36] M. Bruderer and D. Jaksch, New J. Phys. **8**, 87 (2006).
[37] A. Lampo, C. Charalambous, M. Á. García-March, and M. Lewenstein, Phys. Rev. A **98**, 063630 (2018).
[38] J.-B. Yuan, H.-J. Xing, L.-M. Kuang, and S. Yi, Phys. Rev. A **95**, 033610 (2017).
[39] L. Ratschbacher, C. Sias, L. Carcagni, J. M. Silver, C. Zipkes, and M. Köhl, Phys. Rev. Lett. **110**, 160402 (2013).
[40] K. K. Nielsen, L. P. Ardila, G. M. Bruun, and T. Pohl, New J. Phys. **21**, 043014 (2019).
[41] P. Haikka, S. McEndoo, and S. Maniscalco, Phys. Rev. A **87**, 012127 (2013).
[42] M. Schlosshauer, Rev. Mod. Phys. **76**, 1267 (2005).
[43] H.-P. Breuer, E.-M. Laine, J. Piilo, and B. Vacchini, Rev. Mod. Phys. **88**, 021002 (2016).
[44] V. May and O. Kühn, *Charge and Energy Transfer Dynamics in Molecular Systems* (Wiley-VCH, Berlin, 2001).

[45] T. F. Gallagher, *Rydberg Atoms* (Cambridge University Press, Cambridge, UK, 1994).

[46] C. J. Pethik and H. Smith, *Bose-Einstein Condensation in Dilute Gases* (Cambridge University Press, Cambridge, UK, 2002).

[47] C. H. Greene, A. S. Dickinson, and H. R. Sadeghpour, Phys. Rev. Lett. **85**, 2458 (2000).

[48] A. Omont, J. Phys. **38**, 1343 (1977).

[49] M. T. Eiles, J. Phys. B: At. Mol. Opt. Phys. **52**, 113001 (2019).

[50] M. Schlagmüller, Ph.D. thesis, Universität Stuttgart, Stuttgart, Germany, 2016.

[51] M. Flannery, D. Vrinceanu, and V. Ostrovsky, J. Phys. B: At. Mol. Opt. Phys. **38**, S279 (2005).

[52] S. Middelkamp, I. Lesanovsky, and P. Schmelcher, Phys. Rev. A **76**, 022507 (2007).

[53] R. Mukherjee, C. Ates, W. Li, and S. Wüster, Phys. Rev. Lett. **115**, 040401 (2015).

[54] T. Karpiuk, M. Brewczyk, K. Raążewski, A. Gaj, J. B. Balewski, A. T. Krupp, M. Schlagmüller, R. Löw, S. Hofferberth, and T. Pfau, New J. Phys. **17**, 053046 (2015).

[55] S. K. Tiwari and S. Wüster, Phys. Rev. A **99**, 043616 (2019).

[56] M. Schlagmüller, T. C. Liebisch, F. Engel, K. S. Kleinbach, F. Böttcher, U. Hermann, K. M. Westphal, A. Gaj, R. Löw, S. Hofferberth *et al.*, Phys. Rev. X **6**, 031020 (2016).

[57] For the present parameters (Sr atoms at density 4.9×10^{20} m^{-3}), this force could lead to a motion of 3 μm during 30 μs, assuming a relatively large background-density gradient of 5% over 2 μm.

[58] J. B. Balewski, Ph.D. thesis, University of Stuttgart, Stuttgart, Germany, 2014.

[59] K. Bartschat and H. Sadeghpour, J. Phys. B **36**, L9 (2002).

[60] Y. N. Martinez de Escobar, P. G. Mickelson, P. Pellegrini, S. B. Nagel, A. Traverso, M. Yan, R. Côté, and T. C. Killian, Phys. Rev. A **78**, 062708 (2008).

[61] S. Ravets, H. Labuhn, D. Barredo, T. Lahaye, and A. Browaeys, Phys. Rev. A **92**, 020701(R) (2015).

[62] K. Leonhardt, S. Wüster, and J. M. Rost, Phys. Rev. A **93**, 022708 (2016).

[63] H.-P. Breuer, F. Petruccione, *The Theory of Open Quantum Systems* (Oxford University Press, Oxford, UK, 2002).

[64] A. J. Leggett, S. Chakravarty, A. T. Dorsey, M. P. A. Fisher, A. Garg, and W. Zwerger, Rev. Mod. Phys. **59**, 1 (1987).

[65] M. A. Schlosshauer, *Decoherence and the Quantum-to-Classical Transition* (Springer, Berlin, 2007).

[66] I. I. Beterov, I. I. Ryabtsev, D. B. Tretyakov, and V. M. Entin, Phys. Rev. A **79**, 052504 (2009).

[67] S. K. Kanungo, J. D. Whalen, Y. Lu, T. C. Killian, F. B. Dunning, S. Yoshida, and J. Burgdörfer, Phys. Rev. A **102**, 063317 (2020).

[68] C. Hermann-Avigliano, R. C. Teixeira, T. L. Nguyen, T. Cantat-Moltrecht, G. Nogues, I. Dotsenko, S. Gleyzes, J. M. Raimond, S. Haroche, and M. Brune, Phys. Rev. A **90**, 040502(R) (2014).

[69] R. Mukherjee, T. C. Killian, and K. R. A. Hazzard, Phys. Rev. A **94**, 053422 (2016).

[70] A. Arias, G. Lochead, T. M. Wintermantel, S. Helmrich, and S. Whitlock, Phys. Rev. Lett. **122**, 053601 (2019).

[71] E. K. Dietsche, A. Larrouy, S. Haroche, J. M. Raimond, M. Brune, and S. Gleyzes, Nat. Phys. **15**, 326 (2019).

[72] N. Henkel, R. Nath, and T. Pohl, Phys. Rev. Lett. **104**, 195302 (2010).

[73] C. Charalambous, M. A. Garcia-March, A. Lampo, M. Mehboudi, and M. Lewenstein, SciPost Phys. **6**, 010 (2019).

[74] A. Lampo, S. H. Lim, M. Á. García-March, and M. Lewenstein, Quantum **1**, 30 (2017).

[75] M. Mehboudi, A. Lampo, C. Charalambous, L. A. Correa, M. Á. García-March, and M. Lewenstein, Phys. Rev. Lett. **122**, 030403 (2019).

[76] P. Massignan, A. Lampo, J. Wehr, and M. Lewenstein, Phys. Rev. A **91**, 033627 (2015).

[77] C. Charalambous, M. Á. García-March, G. Muñoz-Gil, P. R. Grzybowski, and M. Lewenstein, Quantum **4**, 232 (2020).

[78] M. M. Khan, H. Terças, J. T. Mendonça, J. Wehr, C. Charalambous, M. Lewenstein, and M. A. Garcia-March, Phys. Rev. A **103**, 023303 (2021).

[79] C. Charalambous, M. A. Garcia-March, M. Mehboudi, and M. Lewenstein, New J. Phys. **21**, 083037 (2019).

[80] M. U. Bruderer, Ph.D. thesis, University of Oxford, Oxford, UK, 2008.

[81] H. T. Ng and S. Bose, Phys. Rev. A **78**, 023610 (2008).

[82] M. Streif, A. Buchleitner, D. Jaksch, and J. Mur-Petit, Phys. Rev. A **94**, 053634 (2016).

[83] C. Sabín, A. White, L. Hackermuller, and I. Fuentes, Sci. Rep. **4**, 6436 (2014).

[84] I. S. Gradshteyn and I. M. Ryzhik, *Table of Integrals, Series, and Products* (Academic Press, New York, 2014).

[85] H.-C. Shao and A. F. Starace, Phys. Rev. A **88**, 062711 (2013).

[86] R. Hartmann and W. T. Strunz, J. Chem. Theory Comput. **13**, 5834 (2017).